J. Fluid Mech. (2008), *vol.* 594, *pp.* 307–340.
doi:10.1017/S0022112007009032 Printed in the United Kingdom

Influence of insoluble surfactant on the deformation and breakup of a bubble or thread in a viscous fluid

M. HAMEED[1], M. SIEGEL[2], Y.-N. YOUNG[2], J. LI[3], M. R. BOOTY[2] AND D. T. PAPAGEORGIOU[2]

[1]Division of Mathematics and Computer Science, Unversity of South Carolina Upstate, Spartanburg, SC 29303, USA

[2]Department of Mathematical Sciences and Center for Applied Mathematics and Statistics, NJIT, Newark, NJ 07102, USA

[3]Department of Engineering, University of Cambridge, Cambridge, CB2 1PZ, UK

(Received 9 August 2006 and in revised form 29 August 2007)

The influence of surfactant on the breakup of a prestretched bubble in a quiescent viscous surrounding is studied by a combination of direct numerical simulation and the solution of a long-wave asymptotic model. The direct numerical simulations describe the evolution toward breakup of an inviscid bubble, while the effects of small but non-zero interior viscosity are readily included in the long-wave model for a fluid thread in the Stokes flow limit.

The direct numerical simulations use a specific but realizable and representative initial bubble shape to compare the evolution toward breakup of a clean or surfactant-free bubble and a bubble that is coated with insoluble surfactant. A distinguishing feature of the evolution in the presence of surfactant is the interruption of bubble breakup by formation of a slender quasi-steady thread of the interior fluid. This forms because the decrease in surface area causes a decrease in the surface tension and capillary pressure, until at a small but non-zero radius, equilibrium occurs between the capillary pressure and interior fluid pressure.

The long-wave asymptotic model, for a thread with periodic boundary conditions, explains the principal mechanism of the slender thread's formation and confirms, for example, the relatively minor role played by the Marangoni stress. The large-time evolution of the slender thread and the precise location of its breakup are, however, influenced by effects such as the Marangoni stress and surface diffusion of surfactant.

1. Introduction

The surface-tension driven motion of a stretched droplet or liquid thread suspended in an ambient fluid is a fundamental process in fluid dynamics, and arises in a broad array of applications including emulsion formation, fluid mixing and fibre coating. The efficiency of dispersing two immiscible fluids, for example, depends critically on how readily an elongated drop or fluid thread disintegrates into smaller droplets, see for example Janssen, Boon & Agterof (1994, 1997). Reviews by Stone (1994), Eggers (1997), Quéré (1999) and Basaran (2002), describe recent investigations on the surface-tension-driven instability in droplets, jets and coatings, and discuss their scientific and technological applications.

Theoretical work on the dynamics of liquid threads goes back to the investigations of Rayleigh (1879, 1892), who performed a linear stability analysis for both inviscid and viscous threads surrounded by an inviscid ambient fluid. Rayleigh found that infinitesimal disturbances to a cylindrical thread grow provided the wavelength of the perturbation is greater than the circumference of the thread. This analysis was later generalized by Tomotika (1935) to include the effect of a viscous surrounding fluid. The outer fluid is found not to affect the criterion for instability, but modifies its growth rate.

Nonlinear evolution of a fluid thread eventually leads to its breakup into droplets. Many of the recent studies of the development and breakup of a liquid thread have been motivated by the desire to understand the space–time singularity that results when the radius of the thread tends to zero. Theoretical studies of this topic often make use of one-dimensional or long-wave approximations to the governing equations that are based on the assumption that the thread is long and slender; see e.g. Eggers & Dupont 1994; Papageorgiou 1995; Brenner, Lister & Stone 1996. When the viscosity of the interior thread is sufficiently large, the dynamics in a neighbourhood of pinch-off is found to be universal, that is, independent of initial and boundary conditions. In this case, a combination of careful numerical studies, scaling theories and local similarity solutions has shed much light on the nature of the singularity at pinch-off (see e.g. Eggers 1993; 1995 and references therein, Lister & Stone 1998; Zhang & Lister 1999; Sierou & Lister 2003; McGough & Basaran 2006). In contrast, the dynamics close to pinch-off for an inviscid thread surrounded by a viscous fluid depends on the specific initial and boundary conditions (see Doshi *et al.* 2003; Suryo, Doshi & Basaran 2004).

Surfactants, or surface contaminants, change the interfacial properties of a fluid and are sometimes added to two-phase mixtures or emulsions to control features such as droplet size. The surface tension of a surfactant-coated interface depends on the local concentration of surfactant, which changes owing to flow, surface deformation and surface diffusion of the contaminant. Further, surface tension gradients caused by variations of surfactant concentration give rise to a tangential, or Marangoni, stress acting on the interface, which can in turn substantially alter interfacial evolution and flow.

Experiments show that surfactant can have a significant effect on the stability of a liquid thread (Burkholder & Berg 1974; Zhang & Basaran 1995). A comprehensive linear stability analysis of the influence of surfactant on the evolution of a cylindrical viscous thread surrounded by another viscous fluid was given by Hansen, Peters & Meijer (1999), following an earlier analysis of Whitaker (1976) on a thread in a passive inviscid surrounding. These studies found that surfactant slows the growth rate of disturbances, owing to the lower interfacial tension and to the surface-stiffening or immobilizing effect of Marangoni stress. Timmermans & Lister (2002) revisited the linear stability of a viscous thread coated with insoluble surfactant and clarified the dominant physical balances in certain limits. They also formulated one-dimensional models that describe the nonlinear development of the thread, and presented a simple scaling theory which shows that, close to breakup, surfactant is swept away from the pinching region and thus has little effect on the dynamics at the pinch point. In a parallel study, Craster, Mater & Papageorgiou (2002) derived and studied computationally the nonlinear long-wave evolution equations. They confirmed numerically that surfactant delays pinching, and that as pinchoff is approached, the pinching structures asymptote to those for clean threads. This conclusion has been borne out by McGough & Basaran (2006).

There have been several numerical studies of the influence of surfactant on the deformation and breakup of a drop in an extensional flow, although these are limited to zero Reynolds number. Stone & Leal (1990) consider the case where the ratio $\lambda = \mu_i/\mu$ of interior to exterior viscosity is unity. Milliken, Stone & Leal (1993) extend these calculations to a wider viscosity range, $0.1 \leqslant \lambda \leqslant 10$, and to other flow conditions. They include an example of the evolution of a prestretched drop with $\lambda = 1$ in a quiescent flow that shows the development of smaller droplets separated by long, slender, quasi-stable filaments or threads. The current paper considers such evolution for zero and small viscosity ratio in much greater detail. Kwak & Pozrikidis (2001) present numerical calculations of the influence of surfactant on an infinite thread evolving in Stokes flow, although they mainly focus on viscosity ratios $\lambda > 1$. Ambravaneswaran & Basaran (1999) and Liao, Franses & Basaran (2006) solve the full Navier–Stokes equations numerically to investigate the effect of insoluble surfactant on the pinch-off of a stretched liquid bridge in an inviscid surrounding. Jin, Gupta & Stebe (2006) study numerically the effect of soluble surfactant on the detachment of a viscous drop ejected from a nozzle into a viscous fluid.

Previous studies of surfactant-coated drops and threads have focused mainly on viscous fluids in a passive inviscid surrounding, or on viscosity matched liquids. A major aim of this paper is to consider the influence of surfactant on the evolution of bubbles and threads for zero and small viscosity ratio $\lambda = \mu_i/\mu$ in greater detail. The case $\lambda = 0$ is of particular interest, in view of the result of Doshi *et al.* (2003) that the morphology at pinch-off of a clean or surfactant-free inviscid thread can be controlled by suitable choice of initial and boundary conditions.

Our investigations include numerical simulations of the Navier–Stokes equations for a slender inviscid bubble evolving in a viscous exterior fluid when an insoluble surfactant is present on the bubble surface. We also derive one-dimensional long-wave equations that describe the deformation of an inviscid or slightly viscous thread with surfactant. The long-wave model provides insight into the formation and shape of quasi-stable threads that are observed in the numerical simulations of a collapsing bubble, and allows us to gauge the relative magnitude of the different physical effects that act during the evolution. For the relatively small values of λ considered here, and for small surface diffusion of surfactant, pinching solutions to the long-wave model show that surfactant is not swept away from the pinch point, as is the case for a viscous thread in a passive inviscid surrounding (Craster *et al.* 2002; Timmermans & Lister 2002; McGough & Basaran 2006). The presence of surfactant therefore has the potential to affect local similarity scalings that may occur in a neighbourhood of pinch-off. However, the emphasis here is on the overall morphology of the evolving thread, rather than on uncovering detailed structure in the neighbourhood of the pinch point.

The rest of the paper is organized as follows. The governing equations are given in § 2, where the numerical method is briefly described. In § 3, the results of direct numerical simulation with Reynolds number less than one are presented for the collapse of an elongated bubble with an inviscid interior in a quiescent flow, showing the formation and evolution of a thin thread when the interface is coated with insoluble surfactant. In § 4, a long-wave asymptotic model, which is motivated by the results of the direct numerical simulations, is derived for the evolution of a thread of either small or zero viscosity in the Stokes flow limit. Long-wave equations in the same small viscosity ratio limit have been given previously without surfactant and via more or less heuristic reasoning by Sierou & Lister (2003) and in the inviscid limit by Doshi *et al.* (2003). The derivation here is more systematic, but can be omitted on a first reading, and indicates how higher-order effects might be included in a long-wave

model if desired. The results of numerical solution of the long-wave model are given in § 5. These show a striking similarity with the results of the direct numerical simulations of § 3 in the formation and initial development of a thread of inviscid interior fluid when surfactant is present. In § 6, further detail of the evolution toward pinch-off is considered, as predicted by both the direct numerical simulations and the long-wave model. It is concluded that transport of surfactant, either by advection along the interface or surface diffusion, is critical in determining the precise location of the point at which the thread first pinches off. Concluding remarks are given in § 7.

2. Governing equations

We consider an incompressible, inviscid, neutrally buoyant bubble that is suspended in a viscous Newtonian fluid. It is known that a surfactant-free slender bubble with an initial profile that has a local minimum away from its endpoints subsequently develops a waist or neck there, the radius of which decreases monotonically and tends to zero at finite time, so that the bubble pinches off under the influence of surface tension see e.g. Doshi *et al.* 2003; Suryo *et al.* 2004. We study how surfactant influences the deformation, the development of a thin neck and thread, and the evolution toward pinch-off.

The governing equations for the flow in the exterior fluid are the incompressible Navier–Stokes equations

$$Re(\partial_t + \boldsymbol{u}\cdot\nabla)\boldsymbol{u} = -\nabla p + \nabla^2\boldsymbol{u}, \tag{2.1}$$

$$\nabla\cdot\boldsymbol{u} = 0, \tag{2.2}$$

written in non-dimensional form. The exterior fluid has constant viscosity μ and constant density ρ. Lengths are non-dimensionalized by the radius a of an undeformed spherical bubble of the same volume, and the velocity $\boldsymbol{u}$ is made non-dimensional by a surface, tension-driven value $U = \sigma^*/\mu$, where σ^* is the surface tension of a clean or surfactant-free bubble. Time is then made non-dimensional by a/U, while the pressure both inside the bubble p_i and outside the bubble p are made non-dimensional by $\mu U/a$. The Reynolds number in (2.1) is $Re = Ua/\nu = \sigma^* a\rho/\mu^2$, where ν is the kinematic viscosity of the exterior fluid (note that Re is the inverse square of the Ohnesorge number which is often used in the literature). Since the viscosity of the interior fluid is neglected, the pressure inside the bubble $p_i = p_i(t)$ is a function of time alone, independent of position $\boldsymbol{x}$.

The boundary conditions at the bubble surface are a balance of stress and the kinematic condition. The balance of stress at the interface requires that

$$(p_i - p)\,\boldsymbol{n} + 2\boldsymbol{e}\cdot\boldsymbol{n} = \sigma(\kappa_\theta + \kappa_z)\boldsymbol{n} - \nabla_s\sigma \tag{2.3}$$

on S, in non-dimensional form, where $\boldsymbol{e}$ is the rate of strain tensor, $\boldsymbol{n}$ is the outward unit normal oriented from the interface to the surrounding fluid, κ_θ and κ_z are the principal normal curvatures of S (taken positive for a concave inward surface), and $\nabla_s = \nabla - \boldsymbol{n}(\boldsymbol{n}\cdot\nabla)$ is the surface gradient operator. The non-dimensional surface tension is σ, and the last term in (2.3) is the Marangoni stress, which is zero for a clean or surfactant-free interface. In the presence of a non-uniform distribution of surfactant, however, the surface tension σ varies and the Marangoni stress is non-zero.

The kinematic condition specifies that the interface S, with equation $F(\boldsymbol{x}, t) = 0$, moves with the normal velocity of the neighbouring fluid, and is given by

$$(\partial_t + \boldsymbol{u}\cdot\nabla)F = 0 \tag{2.4}$$

on S.

When surfactant resides on the interface with a surface concentration Γ, the surface tension is reduced from its surfactant-free or clean value. A model for the dependence of interfacial surface tension on surfactant concentration that incorporates a nonlinear dependence of σ on Γ and the fact that there is an upper bound to the surfactant concentration, denoted by Γ_∞, is the Langmuir equation, which has dimensionless form

$$\sigma = 1 + E\ln(1-\Gamma). \tag{2.5}$$

The surface tension σ in (2.3) and (2.5) is non-dimensionalized by its clean or surfactant-free value σ^*, and the surfactant concentration Γ is made dimensionless by Γ_∞. The parameter E is the elasticity number, and is given by $E = R_g T\Gamma_\infty/\sigma^*$, where R_g and T are the gas constant and the uniform temperature. The elasticity number gives a measure of the sensitivity of surface tension to changes in the concentration of surfactant on S.

The Langmuir equation of state has been shown to provide a good fit to experimental data for many fluid–surfactant systems (Chang & Franses 1995) up to values of Γ referred to as the critical micelle concentration (CMC), at which the integrity of the surfactant monolayer is compromised by micelle formation. This leads to a maximum reduction in surface tension from the surfactant-free value σ^* to that attained at CMC σ_{min}, the value of which varies for different fluid–surfactant systems. For example, at an air–water interface with sodium dodecyl sulphate surfactant the reduction σ_{min}/σ^* is modest, close to a half, while for some systems with an aqueous-hydrocarbon interface and specific surfactants, the maximum reduction σ_{min}/σ^* is enhanced to a seventh (Anna & Mayer 2006) or a tenth (De Bruijn 1993).

The above results are reported under equilibrium conditions. Under dynamic conditions, the maximum reduction in surface tension can be further enhanced by a factor that is of the order of a half, owing to the relaxation time associated with restoring the surfactant monolayer to its equilibrium state. An example of such a reduction for dynamic surface tension data with insoluble surfactant, where the relaxation time is of the order of three hours and the dynamic data are approximated well by the Langmuir equation up to (dynamic) CMC, is given by Liao *et al.* (2006).

The evolution of the surface concentration of surfactant Γ is governed by an advection-diffusion equation, which has been derived for a general parametric representation of the interface $\boldsymbol{x} = \boldsymbol{X}(\boldsymbol{\xi}, t)$ in Wong, Rumschitzki & Maldarelli (1996), namely,

$$\left.\frac{\partial\Gamma}{\partial t}\right|_{\boldsymbol{\xi}} - \left.\frac{\partial \boldsymbol{X}}{\partial t}\right|_{\boldsymbol{\xi}}\cdot\nabla_s\Gamma + \nabla_s\cdot(\Gamma\boldsymbol{u}_s) + \Gamma(\kappa_\theta+\kappa_z)\,\boldsymbol{u}\cdot\boldsymbol{n} = \frac{1}{Pe_s}\nabla_s^2\Gamma, \tag{2.6}$$

for an insoluble surfactant, where the surface velocity $\boldsymbol{u}_s = \boldsymbol{u} - (\boldsymbol{u}\cdot\boldsymbol{n})\boldsymbol{n}$ is the projection of $\boldsymbol{u}$ onto the tangent plane, $Pe_s = Ua/D_s$ is the Péclet number for surface diffusion of surfactant and D_s is the surface diffusivity. The first two terms on the left-hand side, containing the time derivatives, taken together are the time derivative $\partial_t\Gamma|_n$ at a point on S that advances with the interface along the normal direction.

Since the interior fluid is incompressible, the total bubble volume V is conserved, and for an inviscid bubble this must be imposed as a further condition that is required in order to close the system, and which implies

$$V = \tfrac{4}{3}\pi. \tag{2.7}$$

A second conserved quantity is the total amount of surfactant, which satisfies the relation

$$\int_S \Gamma \, \mathrm{d}S = 4\pi\chi, \tag{2.8}$$

where $\chi = \Gamma_i/\Gamma_\infty$, and Γ_i is an average over the bubble surface of the initial surfactant concentration. Equation (2.8) is used as a check on the accuracy of the numerical simulations.

In what follows, the bubble shape and flow field are assumed to be axisymmetric in a cylindrical polar coordinate system $(r,\ \theta,\ z)$ in which the bubble axis is aligned with the z-axis. The bubble is also assumed to be symmetric about the plane $z = 0$, and its profile has radius $r = R(z, t)$.

2.1. *Note on the numerical method*

The numerical method uses an arbitrary Lagrangian–Eulerian (ALE) moving mesh to solve the axisymmetric moving-boundary problem. It employs a body-fitted grid, in which the interface is a line of the grid, and dynamic boundary conditions at the interface are incorporated accurately within a finite-volume formulation. ALE methods were first developed in the context of finite-difference and finite-volume methods. Hirt, amsden & Cook (1974, reprinted 1997) summarizes some early work, whereas Donea, Giuliani & Halleux (1982) and Belytschko, Kennedy & Schoeperle (1980) describe extensions in the finite-element setting. A more recent review is given by Donea & Huerta (2003). ALE methods with finite elements and novel meshing strategies have been successfully applied to study drop breakup (see, e.g. Wilkes, Philips & Basaran 1999; Notz, Chen & Basaran 2001; Doshi *et al.* 2003, and references therein).

Since the boundary conditions at the interface are expressed naturally in terms of primitive variables, i.e. velocity and pressure, the ALE method used in this study, which was developed by Li (2006), uses a discretization of the pressure at the centre of a computational cell while the velocity is discretized at the cell corners. In this formulation, boundary conditions on the pressure and velocity gradient immediately outside the interface S are evaluated directly from the stress-balance boundary condition (2.3), and this is similar to the treatment by Ryskin & Leal (1984) in the collocated-grid method. Mass conservation is applied at the cell centre, and fluxes are evaluated by interpolation from the velocity at the cell corners. The resulting nonlinear system of equations expressing overall conservation of mass and momentum is then solved by a projection method. In this way, numerical boundary conditions at the moving interface are evaluated directly from the stress-balance boundary conditions, so as to facilitate improved accuracy in the solution for the exterior flow field.

The interface S is represented by marker points $\boldsymbol{r}_i$, $i = 1, \ldots, N$ which are updated with the normal velocity of S and cubic splines are used to obtain a smooth representation of the surface and to compute its curvature accurately.

Equation (2.6) for the concentration of surfactant Γ is solved using a fractional step, finite-volume method, as in Li (2006). In the first part of the step, the equation

$$\left.\frac{\partial \Gamma}{\partial t}\right|_n + \nabla_s \cdot (\Gamma \boldsymbol{u}_s) = \frac{1}{Pe_s}\nabla_s^2 \Gamma \tag{2.9}$$

is solved using a finite-volume method. Denoting the average of Γ on a surface element $[\boldsymbol{r}_i, \boldsymbol{r}_{i+1}]$ by $\Gamma_{i+1/2} = \int_{\mathbf{r}_i}^{\mathbf{r}_{i+1}} \Gamma \, \mathrm{d}S/\Delta S_{i+1/2}$, where $\Delta S_{i+1/2}$ is the surface area of the element, we update $\Gamma_{i+1/2}$ using a first-order upwind scheme to compute the

convective flux

$$\frac{\left(\Gamma_{i+1/2}^{n+1/2}-\Gamma_{i+1/2}^{n}\right)\Delta S_{i+1/2}^{n}}{2\pi\Delta t}+(R\Gamma u_s)_{i+1}^{n}-(R\Gamma u_s)_{i}^{n}=\frac{1}{Pe_s}\left[\left(R\frac{\partial\Gamma}{\partial s}\right)_{i+1}^{n}-\left(R\frac{\partial\Gamma}{\partial s}\right)_{i}^{n}\right], \tag{2.10}$$

where $u_s=|\mathbf{u}_s|$, R is the axisymmetric interface radius, and s is arclength along $r=R$. The second part of the step updates Γ according to the motion of the interface in the normal direction, that is,

$$\left.\frac{\partial\Gamma}{\partial t}\right|_{n}+\Gamma\left(\kappa_\theta+\kappa_z\right)\boldsymbol{u}\cdot\boldsymbol{n}=0. \tag{2.11}$$

During this part of the step, the total surfactant within each surface element $\int_{\mathbf{r}_i}^{\mathbf{r}_{i+1}}\Gamma\mathrm{d}S$ is conserved, so that the new average concentration is computed as

$$\Gamma_{i+1/2}^{n+1}=\Gamma_{i+1/2}^{n+1/2}\Delta S_{i+1/2}^{n}/\Delta S_{i+1/2}^{n+1}, \tag{2.12}$$

once the marker positions have been updated and the new surface area $\Delta S_{i+1/2}^{n+1}$ has been found. The numerical scheme therefore conserves the total amount of surfactant on S up to round-off error. The flow solver is second-order accurate in space, and the discretization of the equation for Γ in (2.10) is first-order accurate in space. The time update is by explicit Euler and is first-order accurate.

The method has been validated on several problems of bubble dynamics for both steady and unsteady flows, and good agreement with other theoretical, numerical and experimental results has been obtained. See Li (2006) and Li *et al.* (2005) for further details of the numerical method and its validation.

3. Results of numerical simulations

The initial profile for the simulations consists of a dumb-bell shaped bubble which is symmetric in the plane $z=0$, in addition to the axisymmetry about the axis $r=0$. The choice of initial data is motivated by the result (Doshi *et al.* 2003) that a clean slender bubble with a local minimum away from its endpoints will contract and pinch off in finite time.

The particular dumb-bell shape used here is achieved by straining a spherical bubble that is centred at the origin and placed in the extensional flow

$$\boldsymbol{u}=Ca\left(z\boldsymbol{e}_z,-\tfrac{1}{2}r\boldsymbol{e}_r\right), \tag{3.1}$$

where $Ca=Ga/U$ is the capillary number and G is the strain rate of the imposed flow. During the straining motion the surface tension is constant, with $E=0$ in (2.5), so that the interface evolves as though it is free of surfactant. The extent of deformation is characterized by the Taylor deformation number

$$D=\frac{L-B}{L+B}, \tag{3.2}$$

where L and B are, respectively, the bubble half-length in the z-direction and the minimum radius in the r-direction. The initial profile for the simulations below has the bubble shape that is formed under these conditions with the arbitrary choice $Ca=5.87$ and $Re=0.17$ when the deformation number attains the value $D=0.91$ and the aspect ratio is approximately 0.05, at which instant, time is set to $t=0$. This profile $R(z,0)$ has a minimum radius or neck at $z=0$, and is shown by the dashed

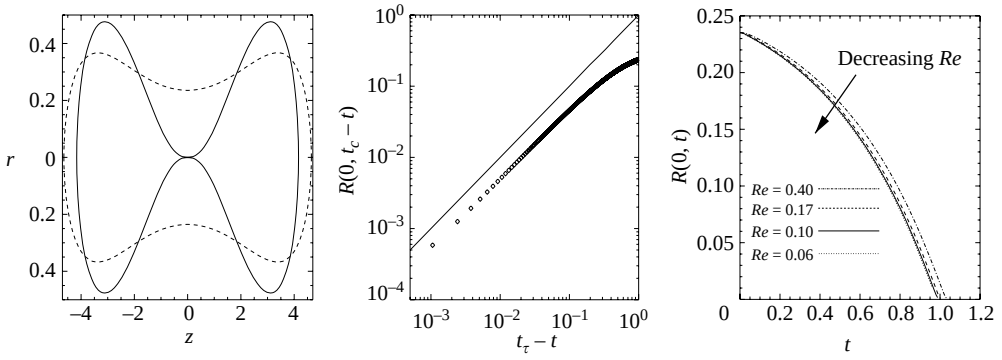

FIGURE 1. (*a*) The dashed curve shows the bubble shape $r = R(z, t)$ at time $t = 0$, and the solid curve shows the shape of the bubble just before pinch-off when it is free of surfactant and $Re = 0.17$. The bubble profile at pinch-off for $|z| \lesssim 2$ is nearly independent of the Reynolds number for $Re \lesssim 1$. (*b*) Log–log plot of the minimum radius $R(0, t)$ versus time to pinch-off $t_c - t$ (markers), where t_c is the pinch-off time. The solid line, shown for comparison, has slope of 1. (*c*) Bubble neck radius $R(0, t)$ as a function of time for values of the Reynolds number $Re \leqslant 0.40$, showing that the evolution is nearly independent of Re for $Re \lesssim 0.25$.

curve in figure 1(*a*). The strain rate and fluid velocity are then instantaneously set to zero, so that $Ca = 0$ and $\boldsymbol{u}(\boldsymbol{x}, 0) = 0$, and the bubble evolves in a quiescent flow for times $t > 0$. At the low Reynolds numbers considered, there is negligible difference in the evolution if at $t = 0$ the imposed flow is set to zero while the fluid velocity for finite $\boldsymbol{x}$ is continuous.

For a bubble of air in glycerine, this profile would be attained by straining a spherical bubble of radius $a \simeq 1.16\,\text{cm}$ at a strain rate $G \simeq 13.64\,\text{s}^{-1}$.

3.1. *Evolution of a clean bubble*

The evolution of a clean or surfactant-free bubble serves as a benchmark for comparison and study of the influence of surfactant. A comprehensive investigation of the evolution of a clean bubble is given in Doshi *et al.* (2003), and we summarize the main features here. When the bubble profile described above evolves in a quiescent flow for $t > 0$, in the surfactant-free state the minimum or neck radius $R(0, t)$ decreases monotonically in time, and the bubble pinches off at $z = 0$ with a locally parabolic minimum at an approximate time $t = 1.0$ for $Re = 0.17$. The bubble profile immediately before pinch-off is shown by the solid curve in figure 1(*a*), for which the Reynolds number takes the same value $Re = 0.17$, used in setting up the initial profile. Figure 1(*b*) shows a log–log plot of the minimum radius as a function of time $t_c - t$ to breakup, where t_c is the pinch-off time. The markers approach a slope of 1, indicating that the thread pinches off with constant velocity. Near pinch-off, the dominant force balance is between normal viscous stress, internal pressure, and capillary pressure (Doshi *et al.* 2003; Suryo *et al.* 2004), as is seen from (4.50) in the long-wave analysis of § 4.

The qualitative features of pinch-off for a clean bubble are independent of Re for values $Re \lesssim 1$. Pinch-off always occurs at $z = 0$ with a single minimum that is locally parabolic. The time at which pinch-off occurs decreases slightly as Re is decreased, as indicated by the evolution of the neck radius $R(0, t)$ shown in figure 1(*c*) for Reynolds numbers in the range from 0.06 to 0.4. The trends in the figure suggest that the pinch-off time converges to a fixed value as $Re \to 0$. The evolution of $R(0, t)$ is seen to be nearly independent of t for Re below $Re \simeq 0.25$. More importantly, the

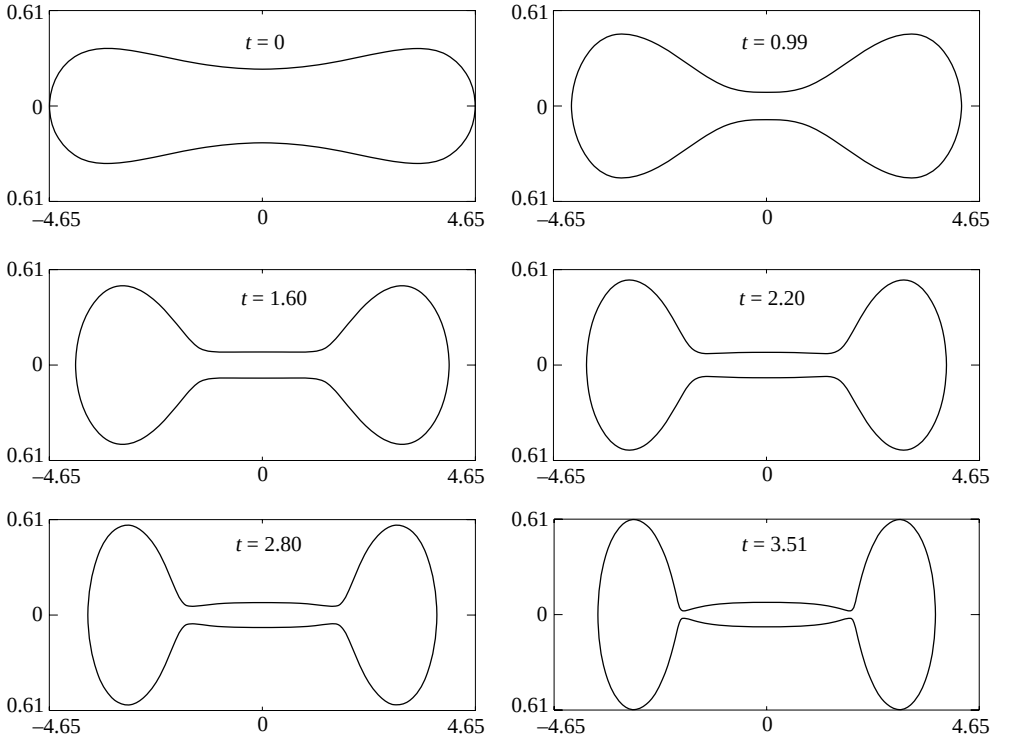

FIGURE 2. The formation of an inviscid thread due to insoluble diffusion-free surfactant. The initial dumb-bell shape is the same as in figure 1(*a*). The bubble collapses radially near $z = 0$ to form a thin thread, which lengthens as its surfactant concentration approaches the saturated value Γ_∞.

final stages of evolution before pinch-off do not show a change in behaviour from a Stokes regime to an inertial viscous regime, as has been shown to occur when a large-viscosity interior fluid is present. The reason for the difference is that, in the latter case, large axial velocities develop in the viscous interior fluid, and inertial terms cannot be neglected in the final stage of pinch-off. This transition from the Stokes to the inertial viscous regime has been shown experimentally in Rothert, Richter & Rehberg (2001) and numerically for a one-dimensional long-wave model in Craster *et al.* (2002). Here the interior fluid is inviscid.

The computations are stopped when the neck radius $R(0, t)$ decreases below 10^{-3}. The results in figures 1(*a*) and 1(*b*) are shown for computations with 128 markers in a quarter-plane, $r > 0$, $z > 0$, and are identical to within the resolution of the figures for computations with 64 markers.

3.2. *Thread formation with insoluble surfactant*

When the same initial bubble shape of figure 1(*a*) is used but the interface is covered with an initial distribution of insoluble surfactant that is diffusion-free, so that $Pe_s = \infty$, a clear difference in evolution toward pinch-off is found. This is distinguished by the formation of a long thin thread of the interior fluid.

A typical example of this is shown in figure 2. Initially, the bubble collapses in a neighbourhood of the minimum to form a short neck near $z = 0$, similar to the surfactant-free evolution of figure 1. In this early stage of the process, the capillary pressure, defined as $p_c = \sigma(\Gamma)/R$, is greater than the internal pressure p_i near $z = 0$.

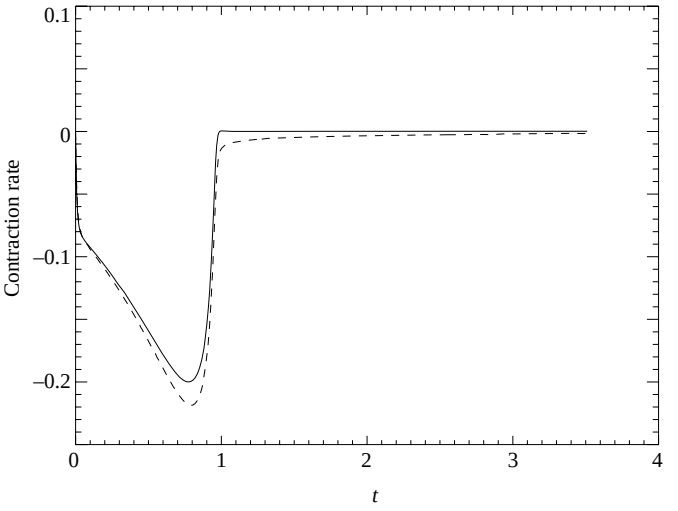

FIGURE 3. Contraction rate $\partial R(0,t)/\partial t$ (dashed line) and the expression on the right-hand side of (3.3) at $z=0$ (solid line) versus time.

However, as the neck forms, the radial contraction and local decrease of surface area causes a high concentration of surfactant to develop around the bubble neck, which greatly decreases the surface tension there. The surface tension is found to decrease sufficiently rapidly relative to the decrease in neck radius that the capillary pressure approaches the pressure of the internal fluid before the neck radius tends to zero. The decrease in neck radius is interrupted when these two forces balance, before pinch-off can occur. We note that the presence of a viscous interior fluid can also cause a transition from a parabolic to a thin thread profile (Doshi *et al.* 2003; Suryo *et al.* 2004).

At later times, the neck lengthens to form a thin thread along the bubble's axis of symmetry, in which the capillary pressure and internal pressure are nearly equal. At its ends, the thread adjoins two parent bubbles via bridges.

The balance of internal and capillary pressures in establishing a steady thin thread is justified in more detail in § 4, where a long-wave asymptotic model is introduced for the evolution of a thread of interior fluid. There it is shown that if ϵ is the small aspect ratio of the initial thread radius to the axial half-wavelength of a periodic disturbance, the ϵ-scaled thread radius $r=\epsilon R(z,t)$ satisfies the equation

$$\frac{\partial R}{\partial t}=\frac{R}{2}\left(p_i-\frac{\sigma(\Gamma)}{R}\right), \tag{3.3}$$

which clearly shows that the thread radius is steady when the internal and capillary pressure are equal.

Figure 3 shows the contraction rate at the neck $(\partial R/\partial t)(0,t)$ (dashed line) together with the right-hand side of (3.3) evaluated at $z=0$ (solid line) as computed from the simulation data. The two curves are close for all times, indicating that the neck radius follows the evolution given by the simplified equation (3.3). The contraction rate is near zero, or more precisely it is less than 10^{-2}, for times $t \gtrsim 1.0$, when a quasi-steady thin thread forms. In contrast, for a clean or surfactant-free interface, the interior pressure cannot equal the large capillary pressure, which grows as $1/R$, and the thread is driven to pinch-off.

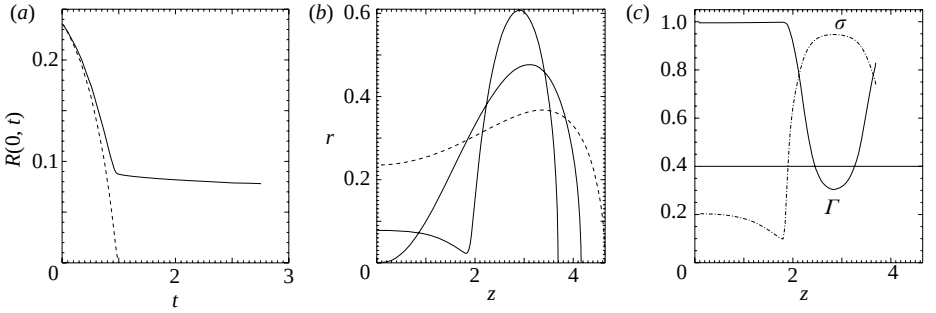

FIGURE 4. (*a*) Radius $R(0, t)$ at the neck as a function of time. Solid line, with surfactant, showing that pinch-off at the neck is interrupted; dashed line, without surfactant. (*b*) Bubble profiles $r = R(z, t)$. The thick solid line shows the surfactant-covered profile with an elongated thread at time $t = 3.51$ and the thin solid line shows the clean bubble at time $t = 0.97$ just before it pinches off at $z = 0$. The dashed line shows the initial bubble profile. (*c*) Surfactant distribution at $t = 0$ (thin solid line), and surfactant distribution (thick line) and surface tension (broken line) at $t = 3.51$.

Simulations have been carried out with both uniform and non-uniform surfactant distributions at time $t = 0$. Although different equilibrium bubble shapes occur for different values of the total amount of surfactant on the bubble surface, results from a large number of simulations show that the spatial distribution of surfactant in the initial conditions is not crucial to the phenomenon of thread formation, which is found to be robust. In the data of figure 2, the distribution of Γ at $t = 0$, Γ_i, is uniform with $\Gamma_i = 0.4$, and the evolution of the bubble shape for $t > 0$ is computed with $E = 0.19$ and $Re = 0.17$.

Further contrast between the evolution for clean and surfactant-covered bubbles is shown in figure 4, using data from the simulations of figure 2. Figure 4(*a*) shows the bubble radius $R(0, t)$ at the mid-point of the bubble profile $z = 0$ versus time t. The radius of the clean bubble, which is shown by the dashed curve, pinches off at $t \simeq 1.0$. Although the radius of the surfactant-covered bubble, shown by the solid curve, is nearly identical in the early stage of its evolution, just before $t \simeq 1.0$ its motion is suddenly interrupted when the radius reaches a near-equilibrium value of $R(0, t) \simeq 0.08$. This is the time at which the capillary pressure and the interior pressure balance at $z = 0$, and marks the onset of formation of the thin thread. Figure 4(*b*) shows the different bubble profiles. The shape of the clean bubble with its locally parabolic minimum (or neck) immediately before pinch-off is given by the thin solid line, whereas the thick solid line shows the surfactant-covered bubble with a well-developed thin thread at time $t = 3.51$, when it has half-length $l \simeq 1.8$. At this instant, the thread aspect ratio is approximately 0.04. The thread radius is not constant in z, and in particular as the thread elongates by radial contraction of the adjacent parent bubble surface, it begins to narrow at the ends, as is also seen in figure 2. Simulations with Pe_s large but finite do not differ appreciably from the results shown with $Pe_s = \infty$. For the surfactant-covered bubble, figure 4(*c*) shows the initial distribution of surfactant $\Gamma_i = 0.4$, given by the thin solid line, whereas at time $t = 3.51$ the surfactant distribution is given by the thick solid line and the surface tension is given by the broken line.

The bubble profile at time $t = 3.51$ is nearly steady, as is the thread radius $R(z, t)$ at fixed z throughout its formation. Figure 4 shows that the surfactant coverage at all points on the thread is within 1% of its maximum value, at which $\sigma = 0$, which is $\Gamma = 0.9948$ with the value of $E = 0.19$ used in the simulation. The surface tension

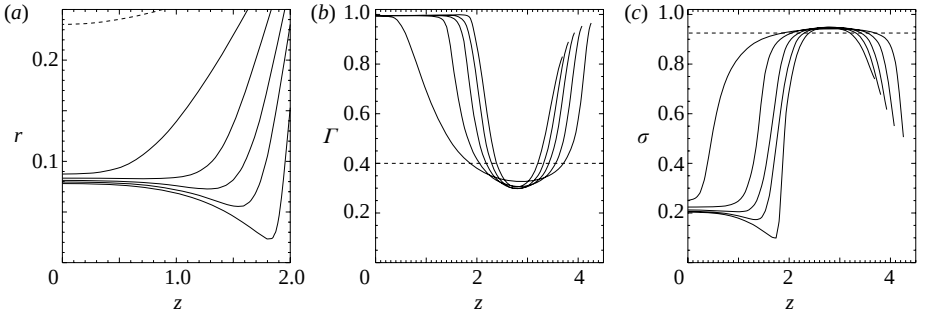

FIGURE 5. Thread evolution for the initial conditions, parameters, and times of figure 2. (*a*) Close-up of the developing thread profile. (*b*) The surfactant concentration $\Gamma(z, t)$. (*c*) The corresponding surface tension $\sigma(z, t)$.

on the thin thread varies from 0.2 at its centre to 0.1 at the constriction. As the thin thread evolves toward pinch-off, the surface tension near the pinch-off point may decrease to values below which the Langmuir equation of state is valid. We return to this point at the end of § 5.1.1.

A magnified view of thread evolution for the initial conditions and parameters of figure 2 is presented in figure 5. Figure 5(*a*) shows the interfacial profiles at a sequence of times, and shows that the thread lengthens by contraction of the adjacent parent bubble. The thin thread is nearly steady; for example, on the interface at $t = 1.6$ there are points on the thread at fixed z with $|z| \lesssim 0.5$ for which $\partial R/\partial t \simeq 0$, while the adjacent parent bubble surface contracts, causing the thread to elongate. Figure 5(*b*) gives the surfactant concentration Γ at the same times as the profiles shown in figure 5(*a*), and figure 5(*c*) shows the corresponding surface tension σ. The value of surface tension at the onset of thread formation is about $\sigma = 0.25$. As the thread elongates, the axial propagation rate of the thread neck junction or constriction decreases.

We have performed simulations for a range of initial surfactant concentration with the elasticity parameter E in the physically representative interval $0.05 < E < 0.4$ (as determined by the experimental data in, for example, Chang & Franses 1995), and find the thin thread typically forms when σ is reduced by a factor of 3 to 10. For example, figure 6 shows $\sigma(z = 0)$ at thread formation versus Γ_i, with other parameters as in figure 2. Thread formation is defined to occur when the capillary pressure σ/R is within 1 % of the interior pressure $p_i(t)$, at which point the radial thread velocity as determined from the right-hand side of (3.3) is less than 0.01. The curves in the figure are obtained from direct numerical simulation and from solutions to the long-wave model of § 4, for similar initial data. The observed values of σ at thread formation are generally within the range of applicability of the Langmuir equation, as noted earlier.

Simulations for the collapse of a surfactant-coated bubble with $Re < 1$ show no indication of a change in behaviour from a Stokes regime to an inertial viscous regime as pinch-off is approached when the interior fluid is inviscid, as noted earlier in the discussion of pinch-off in the surfactant-free case (figure 1(*b*)).

4. Long-wave asymptotic model for a slender thread

The formation of a small-aspect-ratio thread during the collapse of an extended bubble that is observed in the simulations of the previous section motivates us to consider an asymptotic model using a long-wave approximation of the governing equations. In this section we derive such a model, and, since the generalization is straightforward, we include the effect of a small but non-zero viscosity of the

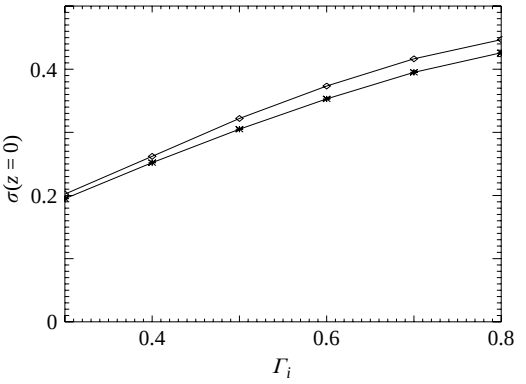

FIGURE 6. Surface tension $\sigma(z=0)$ at thread formation versus Γ_i, with other parameters as in figure 2. Thread formation is defined to occur when $\sigma/R - p_i = 0.01$. $\diamond$, direct numerical simulation with initial conditions as in figure 2; $\times$, crosses long-wave model of §4, for similar initial data.

interior fluid. However, the Reynolds number Re must be set to zero to obtain the simplifications of Stokes flow that are used in the analysis.

Similar models have been considered previously, and the reader may choose to omit the derivation and proceed directly to the result, which appears at (4.52)–(4.55). For example, Sierou & Lister (2003) have thoroughly investigated the dynamics of a slightly viscous thread that is free of surfactant, and the model equations they introduce are equivalent to (4.52) and (4.53) with the surface tension σ_0 constant. Doshi *et al.* (2003) and Suryo *et al.* (2004) have considered the limit of an inviscid interior, for which the model is given by (4.52) and (4.62).

Much of the physical insight for these models can be traced to the observation of Taylor (1964), that for a nearly inviscid interior fluid the motion of the exterior viscous fluid is approximated well by purely radial collapse and dilation. In a cylindrical geometry, the radial velocity near the interface is given by $u \simeq 2g(z,t)/r$ where $g(z,t)$ is a mass source strength, while from the kinematic condition on the interface $u \simeq \partial_\tau R$ where $\tau = t/\epsilon$ is a rescaled time. The motion of the interior fluid is found by a small aspect ratio or lubrication approximation to be Poiseuille flow. When applied to the conditions for continuity of velocity and normal stress at the interface this implies that its evolution is given by (4.52) and (4.53).

In the presence of insoluble surfactant, it turns out that this insight also provides a leading-order approximation to the evolution of surfactant concentration, which with an equation of state gives the closed system (4.52) to (4.55). The derivation below attempts to make the approximation procedure systematic, and confirms that with or without surfactant the tangential stress balance plays a minor role. In other words, despite the presence of surfactant, the Marangoni stress is a higher-order effect, and the role of the Marangoni stress, to reduce gradients in surfactant concentration, is replaced in the long-wave model that is presented here by surface diffusion of surfactant.

Complications introduced by the presence of rounded bubble end-caps, at which the small-slope assumption fails, are avoided by considering a periodic thread as a model of the bubble midsection. We assume the average initial radius b of the thread to be much smaller than the fixed half-length l, and define the small parameter $\epsilon = b/l \ll 1$.

In this section, all lengths are made dimensionless by the half-length l, with the exception of the radial coordinate r inside the thread, which is non-dimensionalized

by b. This is equivalent to introducing a local coordinate $\tilde{r} = O(1)$ such that $r = \epsilon\tilde{r}$. Since the instability is capillary driven, we introduce a rescaled interior pressure $\tilde{p}_i = \epsilon p_i = O(1)$. This is equivalent to non-dimensionalizing the interior thread pressure by σ^*/b, instead of σ^*/l. The remaining non-dimensionalization is the same as in § 2. With these scalings the interface is given by

$$r = \epsilon\tilde{R}(z,t) \quad \text{or equivalently} \quad \tilde{r} = \tilde{R}(z,t), \tag{4.1}$$

where $\tilde{R} = O(1)$.

The formulation follows that of § 2, with Re set to zero in (2.1). An i-subscript is used to denote quantities in the interior fluid, so that if $\lambda = \mu_i/\mu$ is the ratio of interior to exterior viscosity, the momentum and continuity equations for the interior fluid are

$$\nabla p_i = \lambda\nabla^2\boldsymbol{u}_i, \quad \nabla\cdot\boldsymbol{u}_i = 0. \tag{4.2}$$

The boundary conditions on the interface S now include continuity of velocity

$$\boldsymbol{u} = \boldsymbol{u}_i, \tag{4.3}$$

and the continuity of stress boundary condition (2.3) generalizes to become

$$(p_i - p)\boldsymbol{n} + 2(\boldsymbol{e} - \lambda\boldsymbol{e}_i)\cdot\boldsymbol{n} = \sigma(\kappa_\theta + \kappa_z)\boldsymbol{n} - \nabla_s\sigma. \tag{4.4}$$

In cylindrical-polar coordinates, with radial and axial velocity components u and v, the Stokes equations and the incompressibility condition in the thread region $0 < \tilde{r} < \tilde{R}(z,t)$ are

$$\frac{\lambda}{\epsilon}\left[\frac{1}{\tilde{r}}\frac{\partial}{\partial\tilde{r}}\left(\tilde{r}\frac{\partial v_i}{\partial\tilde{r}}\right) + \epsilon^2\frac{\partial^2 v_i}{\partial z^2}\right] = \frac{\partial\tilde{p}_i}{\partial z}, \tag{4.5}$$

$$\lambda\left[\frac{1}{\tilde{r}}\frac{\partial}{\partial\tilde{r}}\left(\tilde{r}\frac{\partial u_i}{\partial\tilde{r}}\right) - \frac{1}{\tilde{r}^2}u_i + \epsilon^2\frac{\partial^2 u_i}{\partial z^2}\right] = \frac{\partial\tilde{p}_i}{\partial\tilde{r}}, \tag{4.6}$$

$$\epsilon\frac{\partial v_i}{\partial z} + \frac{1}{\tilde{r}}\frac{\partial}{\partial\tilde{r}}(\tilde{r}u_i) = 0, \tag{4.7}$$

while in the outer fluid, $r > \epsilon\tilde{R}(z,t)$, they are

$$\frac{1}{r}\frac{\partial}{\partial r}\left(r\frac{\partial v}{\partial r}\right) + \frac{\partial^2 v}{\partial z^2} = \frac{\partial p}{\partial z}, \tag{4.8}$$

$$\frac{1}{r}\frac{\partial}{\partial r}\left(r\frac{\partial u}{\partial r}\right) - \frac{1}{r^2}u + \frac{\partial^2 u}{\partial z^2} = \frac{\partial p}{\partial r}, \tag{4.9}$$

$$\frac{\partial v}{\partial z} + \frac{1}{r}\frac{\partial}{\partial r}(ru) = 0. \tag{4.10}$$

The boundary conditions at infinity are

$$u, v \to 0, \quad p \to 0 \quad \text{as } r \to \infty. \tag{4.11}$$

The tangential and normal components of the stress balance (4.4) on $r = \epsilon\tilde{R}$ are

$$\frac{2}{1+\epsilon^2\tilde{R}'^2}\left[\epsilon\tilde{R}'\frac{\partial u}{\partial r} + \tfrac{1}{2}(1-\epsilon^2\tilde{R}'^2)\left(\frac{\partial u}{\partial z} + \frac{\partial v}{\partial r}\right) - \epsilon\tilde{R}'\frac{\partial v}{\partial z}\right]$$
$$- \frac{2\lambda}{1+\epsilon^2\tilde{R}'^2}\left[\epsilon\tilde{R}'\frac{\partial u_i}{\partial r} + \tfrac{1}{2}(1-\epsilon^2\tilde{R}'^2)\left(\frac{\partial u_i}{\partial z} + \frac{\partial v_i}{\partial r}\right) - \epsilon\tilde{R}'\frac{\partial v_i}{\partial z}\right] = -\frac{\sigma'}{\sqrt{(1+\epsilon^2\tilde{R}'^2)}}, \tag{4.12}$$

and

$$\tilde{p}_i - \frac{2\epsilon\lambda}{1+\epsilon^2\tilde{R}'^2}\left[\frac{\partial u_i}{\partial r} - \epsilon\tilde{R}'\left(\frac{\partial u_i}{\partial z}+\frac{\partial v_i}{\partial r}\right)+\epsilon^2\tilde{R}'^2\frac{\partial v_i}{\partial z}\right]$$
$$-\epsilon p + \frac{2\epsilon}{1+\epsilon^2\tilde{R}'^2}\left[\frac{\partial u}{\partial r} - \epsilon\tilde{R}'\left(\frac{\partial u}{\partial z}+\frac{\partial v}{\partial r}\right)+\epsilon^2\tilde{R}'^2\frac{\partial v}{\partial z}\right]$$
$$= \frac{\sigma}{\tilde{R}\sqrt{(1+\epsilon^2\tilde{R}'^2)}}\left[1-\frac{\epsilon^2\tilde{R}\tilde{R}''}{(1+\epsilon^2\tilde{R}'^2)}\right]. \tag{4.13}$$

Here and elsewhere a prime denotes a partial derivative with respect to z. The surface tension σ is given by the nonlinear equation of state (2.5).

The surfactant evolution equation (2.6) takes the form

$$\frac{\partial\Gamma}{\partial t}+\frac{1}{\tilde{R}\sqrt{(1+\epsilon^2\tilde{R}'^2)}}\frac{\partial}{\partial z}\left[\frac{\tilde{R}\Gamma}{\sqrt{(1+\epsilon^2\tilde{R}'^2)}}(\epsilon u\tilde{R}'+v)\right]-\frac{\epsilon^2R'}{1+\epsilon^2R'^2}\frac{\partial\tilde{R}}{\partial t}\frac{\partial\Gamma}{\partial z}$$
$$+\frac{\Gamma(u-\epsilon\tilde{R}'v)}{\epsilon\tilde{R}(1+\epsilon^2\tilde{R}'^2)}\left[1-\frac{\epsilon^2\tilde{R}\tilde{R}''}{1+\epsilon^2\tilde{R}'^2}\right]=\frac{1}{Pe_s}\left[\frac{1}{\tilde{R}\sqrt{(1+\epsilon^2\tilde{R}'^2)}}\frac{\partial}{\partial z}\left(\frac{\tilde{R}}{\sqrt{(1+\epsilon^2\tilde{R}'^2)}}\frac{\partial\Gamma}{\partial z}\right)\right], \tag{4.14}$$

on $r=\epsilon\tilde{R}$, where the coordinate α of (2.6) has been set to $\alpha=z$ and now the surface Péclet number $Pe_s=\sigma_0 l/D_s\mu$.

The kinematic condition is

$$u=\epsilon(\tilde{R}_t+v\tilde{R}') \quad \text{on} \quad r=\epsilon\tilde{R}, \tag{4.15}$$

while continuity of velocity is unchanged from (4.3). Conservation of the thread volume (2.7) and of the total amount of surfactant (2.8) are written in non-dimensional form as

$$\int_{-1}^{1}\tilde{R}^2\,\mathrm{d}z=2, \tag{4.16}$$

$$\int_{-1}^{1}\Gamma\tilde{R}\sqrt{(1+\epsilon^2\tilde{R}'^2)}\,\mathrm{d}z=\chi, \tag{4.17}$$

where we recall that $\chi=\Gamma_i/\Gamma_\infty$.

Below, we derive asymptotic equations describing the evolution in the limit of small ϵ.

4.1. *Flow outside the thread*

Evolution of the thread surface is accompanied by a flow in the exterior fluid. Following, for example, Acrivos & Lo (1978) and Buckmaster (1972), we describe the flow by introducing point forces or Stokeslets, with distribution $f\boldsymbol{e}_z$, and point mass sources, with distribution g, along the thread axis $r=0$ for $-\infty<z<\infty$. In terms of these distributions,

$$u=r(I_{1,3}(f)+I_{0,3}(g)), \tag{4.18}$$
$$v=I_{0,1}(f)+I_{2,3}(f)+I_{1,3}(g), \tag{4.19}$$
$$p=2I_{1,3}(f), \tag{4.20}$$
$$\text{where } I_{m,n}(\phi)=\int_{-\infty}^{\infty}\phi(\xi)\frac{(z-\xi)^m}{(r^2+(z-\xi)^2)^{n/2}}\,\mathrm{d}\xi. \tag{4.21}$$

We require that $\int_{-1}^{1} f\,\mathrm{d}z = \int_{-1}^{1} g\,\mathrm{d}z = 0$, since there is no net force acting on the thread and no net mass source inside it, respectively. Expressions (4.18)–(4.21) provide an exact solution of the Stokes equations (4.8)–(4.10) and the far-field condition (4.11) for $r \geqslant \epsilon\tilde{R}(z,t)$.

The problem is now to find Stokeslet and mass source distributions f and g, the components of the velocity inside the thread u_i and v_i, and the surfactant concentration Γ, or equivalently the surface tension, such that the boundary conditions are satisfied to leading order in ϵ on the free interface. The components of the velocity gradient are given by differentiating equations (4.18) and (4.19), and are

$$\frac{\partial u}{\partial r} = I_{1,3}(f) - 3r^2 I_{1,5}(f) + I_{0,3}(g) - 3r^2 I_{0,5}(g), \tag{4.22}$$

$$\frac{\partial u}{\partial z} = r(I_{0,3}(f) - 3I_{2,5}(f) - 3I_{1,5}(g)), \tag{4.23}$$

$$\frac{\partial v}{\partial r} = -r(I_{0,3}(f) + 3I_{2,5}(f) + 3I_{1,5}(g)), \tag{4.24}$$

$$\frac{\partial v}{\partial z} = I_{1,3}(f) - 3I_{3,5}(f) + I_{0,3}(g) - 3I_{2,5}(g). \tag{4.25}$$

To find exterior flow quantities on the interface in terms of f and g, the dominant contribution of the integral $I_{m,n}(\cdot)$ is required for $r = \epsilon\tilde{R}$ and z in the principal period $[-1, 1]$, which is calculated as follows. First, decompose

$$I_{m,n}(\phi) = \int_{-d}^{d} \phi(\xi)\frac{(z-\xi)^m}{(r^2+(z-\xi)^2)^{n/2}}\,\mathrm{d}\xi + J_{m,n}(\phi), \tag{4.26}$$

where $J_{m,n}(\phi)$ denotes the contribution to $I_{m,n}$ from integrating over the region $\xi \in (-\infty, -d) \cup (d, \infty)$, for any $d > 1$. The intervals of integration in (4.26) are chosen so that $J_{m,n}$ has a bounded integrand when $r \to 0$ for $z \in [-1, 1]$. Convergence of the infinite integral $J_{m,n}$ for $n \geqslant m+2$ follows from the ξ^{m-n} decay of the integrand, while convergence of the infinite integrals $J_{0,1}(\phi)$ and $J_{2,3}(\phi)$ is demonstrated by assuming that ϕ has a primitive Φ, which must be bounded in view of the periodicity of ϕ and the identity $\int_{-1}^{1} \phi\,\mathrm{d}\xi = 0$. Therefore, integration by parts can be employed to rewrite $J_{0,1}(\phi)$ and $J_{2,3}(\phi)$ in terms of an infinite integral with ξ^{-2} decay of the integrand, from which their convergence follows. Now, since each $J_{m,n}$ has a bounded integrand, it represents an at most $O(\phi)$ contribution to $I_{m,n}$, and this is found to be of higher order than the contribution from the first term on the right-hand side of (4.26). The expansion of this first integral term in (4.26) is performed following the procedure given by Handelsman & Keller (1967) and Hinch (1991). A summary is given in Booty & Siegel (2005).

When the dominant part of each expansion is included, the exterior fluid velocities, pressure and velocity gradient evaluated on the interface $r = \epsilon\tilde{R}$ are given by

$$\frac{\partial u}{\partial r} = -2\ln(1/\epsilon)f'(z) - \frac{2g(z)}{\epsilon^2\tilde{R}^2} + \cdots, \tag{4.27}$$

$$\frac{\partial u}{\partial z} + \frac{\partial v}{\partial r} = -\frac{4f}{\epsilon\tilde{R}} + \frac{4g'}{\epsilon\tilde{R}} + \cdots, \tag{4.28}$$

$$\frac{\partial v}{\partial z} = 4\ln(1/\epsilon)f'(z) - 2\ln(1/\epsilon)g'' + \cdots, \tag{4.29}$$

$$u = -2\epsilon\ln(1/\epsilon)f'\tilde{R} + \frac{2g}{\epsilon\tilde{R}} + \cdots, \tag{4.30}$$

$$v = 4\ln(1/\epsilon) f - 2\ln(1/\epsilon) g' + \ldots, \tag{4.31}$$

$$p = -4\ln(1/\epsilon) f' + \cdots. \tag{4.32}$$

Here and elsewhere, an ellipsis denotes terms in an expansion that are of higher order.

4.2. *Flow inside the thread and the model equations*

The interior pressure $\tilde{p}_i$ and its derivative $\tilde{p}_i'$ are $O(1)$ when the scales for capillary-driven flow defined above (4.1) are used. Inspection of the axial momentum equation (4.5) then shows that Poiseuille flow or plug flow ensues in the thread interior if, respectively,

$$\frac{\lambda}{\epsilon} v_i \sim 1 \quad \text{or} \quad \frac{\lambda}{\epsilon} v_i \gg 1. \tag{4.33}$$

Here we consider the Poiseuille flow scaling (4.33*a*), which applies for an inviscid or nearly inviscid interior fluid. In this case, the continuity equation (4.7) implies that

$$u_i \sim \frac{\epsilon^2}{\lambda}. \tag{4.34}$$

Estimates are applied to the boundary conditions to determine scalings for the other dependent variables. Consider first the tangential stress balance (4.12). We use the scalings (4.33*a*) and (4.34) and recall that $\partial/\partial r \sim 1/\epsilon$ for thread quantities (i.e. with subscript i) to deduce that the largest term within the second pair of square brackets in (4.12) is $\lambda(\partial v_i/\partial r)$, which is $O(1)$. The leading-order contribution from external flow quantities is determined from (4.27)–(4.29), from which we find that the tangential stress balance takes the form

$$4\left\{-\frac{f}{\epsilon\tilde{R}} + \frac{g'}{\epsilon\tilde{R}} - \frac{g\tilde{R}'}{\epsilon\tilde{R}^2} + \cdots\right\} - \lambda\left\{\frac{\partial v_i}{\partial r} + \cdots\right\} = -\sigma' + \cdots. \tag{4.35}$$

Continuity of the radial and axial components of velocity implies, via (4.30)–(4.31), that on S

$$u_i|_S = -2\epsilon \ln\frac{1}{\epsilon} f'\tilde{R} + \frac{2g}{\epsilon\tilde{R}} + \cdots \tag{4.36}$$

$$v_i|_S = 4\ln\frac{1}{\epsilon} f - 2\ln\frac{1}{\epsilon} g' + \cdots, \tag{4.37}$$

If we now recall that inside the thread $u_i \sim \epsilon^2/\lambda$ and $v_i \sim \epsilon/\lambda$, then inspection of (4.35)–(4.36) shows that a consistent scaling is to set $f, g \sim \epsilon$ for a balance in (4.35), and $\lambda \sim \epsilon^2$ for a balance in (4.36). The axial velocity v_i is then $O(1/\epsilon)$ inside the thread, while (4.37) implies that at this leading order the profile for v_i is zero on the interface S, where in fact $v_i|_S = O(\epsilon\ln(1/\epsilon))$. We therefore introduce order-one quantities λ_0, f_0, g_0, v_{i0}, etc. such that

$$\lambda = \epsilon^2\lambda_0 + \cdots, \quad f = \epsilon f_0 + \cdots, \quad g = \epsilon g_0 + \cdots, \tag{4.38}$$

$$v_i = \frac{1}{\epsilon} v_{i0} + \cdots, \quad u_i = u_{i0} + \cdots, \quad \tilde{p}_i = p_{i0} + \cdots, \tag{4.39}$$

$$\Gamma = \Gamma_0 + \cdots, \quad \sigma = \sigma_0 + \cdots, \quad \tilde{R} = R_0 + \cdots. \tag{4.40}$$

Inside the thread region, the leading-order problem yields lubrication-type equations. Specifically, from (4.6) we have

$$\frac{\partial p_{i0}}{\partial \tilde{r}} = 0, \tag{4.41}$$

so that $p_{i0} = p_{i0}(z, t)$. Equations (4.5) and (4.7) then imply, respectively,

$$\frac{\lambda_0}{\tilde{r}}\frac{\partial}{\partial \tilde{r}}\left(\tilde{r}\frac{\partial v_{i0}}{\partial \tilde{r}}\right) = \frac{\partial p_{i0}}{\partial z}, \quad \frac{\partial v_{i0}}{\partial z} + \frac{1}{\tilde{r}}\frac{\partial}{\partial \tilde{r}}(\tilde{r}u_{i0}) = 0. \tag{4.42}$$

The solution that is bounded at $\tilde{r} = 0$ is

$$\lambda_0 v_{i0} = \frac{\tilde{r}^2 p'_{i0}}{4} + B(z, t), \tag{4.43}$$

$$\lambda_0 u_{i0} = -\frac{\tilde{r}^3 p''_{i0}}{16} - \frac{\tilde{r}B'(z, t)}{2}, \tag{4.44}$$

where we have introduced the function of integration $B(z, t)$, which is to be determined.

The relations (4.27)–(4.32) and (4.43)–(4.44) together with the scalings (4.38)–(4.40) are now used to satisfy the conditions of continuity of velocity and stress across the interface.

Continuity of axial velocity implies, via (4.37) and (4.43), that on S

$$v_{i0}|_S = \frac{1}{\lambda_0}\left(\frac{R_0^2 p'_{i0}}{4} + B\right) = O\left(\epsilon^2 \ln\frac{1}{\epsilon}\right), \tag{4.45}$$

so that

$$B = -\frac{R_0^2 p'_{i0}}{4}. \tag{4.46}$$

When this expression for B is used, continuity of radial velocity implies, via (4.36) and (4.44), that on S

$$u_{i0}|_S = \frac{1}{16\lambda_0 R_0}\left(R_0^4 p'_{i0}\right)' = \frac{2g_0}{R_0}. \tag{4.47}$$

In the kinematic condition (4.15), since $u_i|_S$ is $O(1)$ we introduce a rescaled time τ such that

$$t = \epsilon\tau, \tag{4.48}$$

where τ is an order-one quantity, so that to leading order, the kinematic condition becomes

$$\frac{\mathrm{d}R_0}{\mathrm{d}\tau} = u_{i0}|_S = \frac{2g_0}{R_0}. \tag{4.49}$$

The normal viscous stress is dominated by the external velocity gradient $\partial u/\partial r \sim -2\epsilon g_0/r^2$, which, from (4.13) balances the internal and capillary pressure, to give the normal stress balance

$$p_{i0} - \frac{4g_0}{R_0^2} = \frac{\sigma_0}{R_0}. \tag{4.50}$$

Substituting (4.43) for the internal axial velocity into (4.35) we find that the leading-order tangential stress balance is given by

$$-\frac{4f_0}{R_0} + \frac{4g'_0}{R_0} - \frac{4g_0 R'_0}{R_0^2} - \tfrac{1}{2}R_0 p'_{i0} = -\sigma'_0. \tag{4.51}$$

An evolution equation for R_0 is found by eliminating g_0 between the kinematic condition (4.49) and the normal stress balance (4.50), to give

$$\frac{\partial R_0}{\partial \tau} = \frac{R_0}{2}\left(p_{i0} - \frac{\sigma_0}{R_0}\right), \tag{4.52}$$

while an equation for p_{i0} is found by eliminating g_0 between the expression (4.47) for continuity of radial velocity and (4.50) for the normal stress balance, namely

$$\frac{1}{8R_0}(R_0^4 p_{i0}')' = \lambda_0(p_{i0}R_0 - \sigma_0). \tag{4.53}$$

Equations (4.52) and (4.53) govern the leading-order evolution of the thread when the spatial distribution of surfactant Γ_0, or equivalently σ_0, is known.

An equation for the evolution of Γ is derived from (2.6) and its expression in cylindrical coordinates (4.14). With the rescaled time τ of (4.48) and scalings (4.39)–(4.40), the nearly radial collapse of the external fluid implies that the transport terms on the left-hand side of (2.6) are approximated by $\Gamma(\kappa_\theta + \kappa_z)\boldsymbol{u}\cdot\boldsymbol{n} \simeq \Gamma_0 u_{i0}|_S/\epsilon R_0$. Use of the kinematic condition (4.49) then gives the leading-order expression for conservation of surfactant,

$$\frac{\partial \Gamma_0}{\partial \tau} + \frac{\Gamma_0}{R_0}\frac{\partial R_0}{\partial \tau} = \frac{1}{Pe_0}\frac{1}{R_0}\frac{\partial}{\partial z}\left(R_0\frac{\partial \Gamma_0}{\partial z}\right), \tag{4.54}$$

where we have introduced a rescaled Péclet number $Pe_0 = Pe_s/\epsilon$. This is appended by an equation of state, such as the Langmuir equation (2.5)

$$\sigma_0 = 1 + E\ln(1-\Gamma_0). \tag{4.55}$$

The closed system of equations (4.52)–(4.55) for the evolution of R_0, p_{i0}, Γ_0 and σ_0 is the main result of this section.

We note that the relation for the tangential stress balance (4.51) determines the Stokeslet density $f_0(z,t)$ once the solution of the system (4.52)–(4.55) is known, where from (4.49), $g_0 = R_0\partial_\tau R_0/2$, and in this sense the tangential stress balance decouples from the system. In particular, the decoupling implies that the Marangoni term (i.e. the right-hand side of (4.51)) does not enter into the leading-order dynamics for the evolution of the thread, although the Marangoni term would appear in higher-order corrections to the dynamics and, as an expression for $f_0(z,t)$, (4.51) would be needed to find the small $O(\epsilon\ln(1/\epsilon))$ axial velocity and pressure of the exterior flow, if required.

We also emphasize the result that inside the thread the velocity profile is of Poiseuille type, with leading-order axial component at order $O(1/\epsilon)$ given from (4.39), (4.43) and (4.46) by

$$v_i = \frac{p_{i0}'}{4\epsilon\lambda_0}(\tilde{r}^2 - R_0^2) + \cdots, \tag{4.56}$$

which vanishes on the interface $\tilde{r} = R_0$. Outside but near the thread, the state of nearly radial collapse and dilation is seen from (4.18), (4.30) and (4.38), which show that the radial velocity is given by $u \sim 2\epsilon g_0/r$, which is $O(1)$ on and within an ϵ-neighbourhood of the interface, while the axial velocity in the same region is small and, from (4.31) and (4.38), $O(\epsilon\ln(1/\epsilon))$. The motion of fluid points on the thread surface is thus purely radial to leading order in ϵ. These features predicted by the long-wave dynamics are validated by the direct numerical simulations, which are revisited in § 6.

We conclude this section with some remarks. First, for $\lambda_0 > 0$, the evolution equations (4.52) to (4.55) conserve the thread volume and total amount of surfactant automatically. Conservation of volume follows from (4.52) and (4.53), which give

$$\frac{\mathrm{d}}{\mathrm{d}\tau}\int_{-1}^{1} R_0^2\,\mathrm{d}z = \int_{-1}^{1} R_0(p_{i0}R_0 - \sigma_0)\,\mathrm{d}z = \int_{-1}^{1}\frac{1}{8\lambda_0}\left(R_0^4 p_{i0}'\right)'\mathrm{d}z = 0, \tag{4.57}$$

by periodicity. Similarly, from (4.54), it follows that

$$\frac{\mathrm{d}}{\mathrm{d}\tau}\int_{-1}^{1}\Gamma_0 R_0\,\mathrm{d}z = 0, \tag{4.58}$$

which is the leading-order statement of conservation of surfactant per (4.17). The requirement that $\int_{-1}^{1} g_0\,\mathrm{d}z = 0$ follows immediately from (4.47), and the requirement that $\int_{-1}^{1} f_0\,\mathrm{d}z = 0$ follows on eliminating σ_0 between (4.50) and (4.51) to find that $f_0 = 1/8(R_0^2 p_{i0})'$.

Secondly, we find that with no surface diffusion of surfactant, $Pe_0 = \infty$, (4.54) implies that

$$\frac{\partial}{\partial\tau}(\Gamma_0 R_0) = 0, \tag{4.59}$$

so that,

$$\Gamma_0 = \frac{C(z)}{R_0}, \tag{4.60}$$

where $C(z)$ is a time-independent function determined by the initial conditions. Equation (4.60) implies that for a thread to pinch-off at a point, Γ_0 must tend to infinity there. However, prior to this singularity in Γ_0 developing, the surface tension becomes sufficiently small that the equation of state is no longer valid, and additional effects such as surfactant solubility and micelle formation, which are neglected here, become important. In the numerical study of § 5, we see that a thread coated with an insoluble diffusion-free surfactant that evolves according to the leading-order long-wave equations is such that R_0 remains bounded away from zero.

4.2.1. *The limit of an inviscid thread ($\lambda_0 = 0$)*

An important special case is that of an inviscid thread, for which $\lambda_0 = 0$. Letting $\lambda_0 \to 0$ in (4.53) gives

$$\frac{1}{8R_0}\left(R_0^4 p_{i0}'\right)' = 0, \tag{4.61}$$

which implies that $p_{i0}' = \gamma(t)/R_0^4$ where $\gamma(t)$ is a function of time alone. A further integration over $z \in [-1, 1]$ and periodicity of the boundary conditions implies that the function $\gamma(t)$ vanishes, so that $p_{i0} = p_{i0}(t)$, independent of z. However, (4.53) then implies no further information about the evolution of the interior pressure.

In the inviscid limit, a separate relation that determines the interior pressure must be found, and it is obtained from the condition of volume conservation (4.16). The time-derivative of (4.16) implies that $\int_{-1}^{1} R_0\partial_\tau R_0\,\mathrm{d}z = 0$, and together with (4.52), the fact that p_{i0} is independent of z, and a further use of (4.16), this gives the result

$$p_{i0} = \frac{1}{2}\int_{-1}^{1}\sigma_0 R_0\,\mathrm{d}z. \tag{4.62}$$

4.2.2. *Linear stability*

In this subsection we compare the linearized behaviour of the long-wave equations with that of the governing equations in the Stokes flow limit. Specifically, we consider the linear stability of a disturbance to an initially cylindrical thread coated with a uniform distribution of insoluble surfactant, surrounded by a viscous fluid. For small perturbations from an equilibrium surfactant concentration Γ_i, the equation of state

(2.5) or (4.55) can be approximated by

$$\sigma = \sigma_i - E_0 \frac{\Gamma - \Gamma_i}{\Gamma_i}, \tag{4.63}$$

where $\sigma_i = \sigma(\Gamma_i)$ and $E_0 = -(\partial\sigma/\partial\Gamma)|_{\Gamma_i}\,\Gamma_i$. It is convenient to rescale the surface tension by σ_i and the surfactant concentration by Γ_i, so that the dimensionless surface tension becomes

$$\sigma = 1 - \beta\tilde{\Gamma}, \tag{4.64}$$

where $\tilde{\Gamma} = (\Gamma - \Gamma_i)/\Gamma_i$ and $\beta = E_0/\sigma_i$. Note that for a surfactant-free interface $\beta = 0$.

The linearized version of the long-wave equations (4.52) to (4.55) about the uniform state with $R_0 = 1$ and $p_{i0} = 1$, admits normal mode solutions proportional to $\mathrm{e}^{ikz+\omega t}$ with growth rate ω given by

$$\omega(k) = \frac{k^2}{4(8\lambda_0 + k^2)}\left\{(1-\beta) - \frac{2}{Pe_0}(8\lambda_0 + k^2) \pm \left[(1-\beta)^2 + \frac{4}{Pe_0}(1+\beta)(8\lambda_0 + k^2) + \frac{4}{Pe_0^2}(8\lambda_0 + k^2)^2\right]^{1/2}\right\}, \tag{4.65}$$

where k is the wavenumber made dimensionless by the thread half-length l. For a diffusion-free surfactant $Pe_0 = \infty$, and the two roots of the dispersion relation simplify to

$$\omega(k) = 0, \quad \omega(k) = \frac{(1-\beta)k^2}{2(8\lambda_0 + k^2)}, \tag{4.66}$$

that is, there is one marginally stable branch and one branch that is unstable (stable) when $\beta < 1$ ($\beta > 1$). In contrast, when $Pe_0 < \infty$, (4.65) has a stable and an unstable branch for each k.

A comprehensive linear stability analysis of a viscous filament surrounded by another viscous fluid in the presence of soluble surfactant has been given by Hansen *et al.* (1999). Equation (5.3) of that paper gives a characteristic equation for linear disturbances to a uniform state in the limit of zero Reynolds number. When we take the limit of zero bulk diffusivity, corresponding to insoluble surfactant, and express the equation in terms of the dimensionless parameters defined in § 4, it takes the form

$$\omega\left\{(\lambda-1)[G^2(\tilde{k}) - 1 - \tilde{k}^2]\tilde{k}F'(\tilde{k}) + \lambda(\lambda-1)[F^2(\tilde{k}) - 1 - \tilde{k}^2]\tilde{k}G'(\tilde{k}) + \lambda[G(\tilde{k}) + F(\tilde{k})]^2 + \frac{\beta}{2}\left(\omega + \frac{\tilde{k}^2}{Pe_H}\right)^{-1}(1+\tilde{k}^2)\left[\lambda\tilde{k}G'(\tilde{k}) + \tilde{k}F'(\tilde{k})\right]\right\} = \frac{(1-\tilde{k}^2)}{2}\left[\lambda\tilde{k}G'(\tilde{k}) + \tilde{k}F'(\tilde{k}) + \frac{\beta}{2}\left(\omega + \frac{\tilde{k}^2}{Pe_H}\right)^{-1}\tilde{k}G'(\tilde{k})\tilde{k}F'(\tilde{k})\right]. \tag{4.67}$$

Here, $\tilde{k}$ is the wavenumber based on the thread radius, $F(\tilde{k}) = \tilde{k}I_0(\tilde{k})/I_1(\tilde{k})$, $G(\tilde{k}) = \tilde{k}K_0(\tilde{k})/K_1(\tilde{k})$ and I_n and K_n are modified Bessel functions of the first and second kind (of order n).

A straightforward but lengthy calculation, putting $\tilde{k} = \epsilon k$, $Pe_H = \epsilon^2 Pe_0$ and $\lambda = \epsilon^2\lambda_0$ in (4.67), verifies that the roots of the long-wave model (4.65) are the same as those of the characteristic equation (4.67) at leading order in ϵ, with a difference that is $O(\epsilon^2 \ln(1/\epsilon))$.

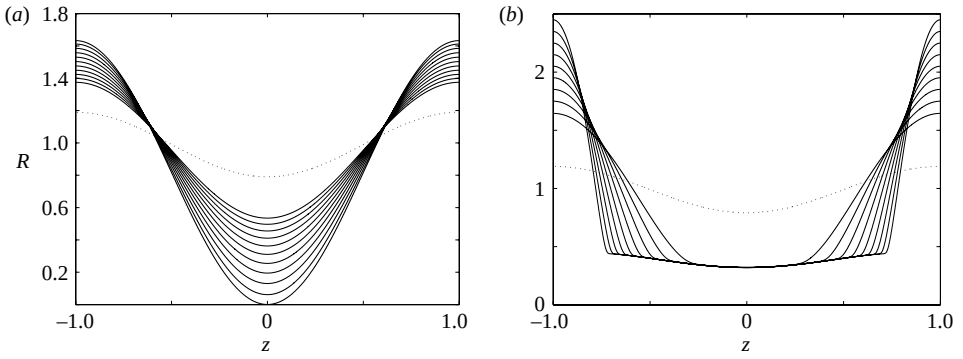

FIGURE 7. Numerical solutions of the long-wave equations with $\lambda_0 = 0$ and $Pe_0 = \infty$. (*a*) Evolution of a clean interface shown for $t = 0$ and from $t = 1.55$ to $t = 3.05$ in increments of $\Delta t = 0.15$. (*b*) Evolution of an interface coated with an initially uniform distribution of diffusion-free insoluble surfactant with $\Gamma_i = 0.4$, shown for $t = 0$ and from $t = 4$ to $t = 12$ in increments of $\Delta t = 1$. The dashed curve denotes the initial profile.

5. Numerical solution of the long-wave model

The long-wave model given by (4.52) – (4.55) is found to capture the essential features of the collapse of a prestretched bubble, including the formation of a quasi-steady thin thread, as is shown by the results of the model's numerical solution described in this section. The model also provides insight into the dominant physical mechanisms that are responsible for thin thread formation, the large-time occurrence of a constriction at the thread ends, and the evolution toward pinch-off of the interface.

Equations (4.52)–(4.55) are solved using a finite-difference method. The initial data are chosen to be similar to those of the direct numerical simulations of § 3, for which the initial profile is shown in figures 1(*a*) and 2. For example, as in § 3, the initial surfactant concentration is uniform with $\Gamma_i = 0.4$ and the elasticity number is $E = 0.19$. The zero-subscript on the dependent variables R, p_i, Γ and σ of the long-wave model are now omitted, and the initial profile is given by $R(z, 0) = a - \sqrt{2(1 - a^2)}\cos \pi z$ with $a = 0.9888$ to give a profile that is reminiscent of the dumb-bell shaped bubble of figure 1(*a*) up to its maximum radius, and where the coefficient multiplying the cosine term is determined from the volume constraint (4.16). The initial pressure $p_i(z, 0)$ then follows from (4.53) when the viscosity ratio $\lambda_0 > 0$ and from (4.62) when $\lambda_0 = 0$.

The thread volume and the total amount of surfactant over a spatial period $z \in [-1, 1]$, which are conserved quantities proportional to the integrals on the left-hand sides of (4.57) and (4.58), are monitored as a check on the simulations, and remain within 10^{-5} to 10^{-6} of their initial values.

5.1. *The inviscid limit ($\lambda_0 = 0$)*

Figure 7 compares the evolution predicted by the long-wave equations for a clean interface and one that contains an initially uniform distribution of insoluble surfactant that is diffusion free ($Pe_0 = \infty$).

The main features of the evolution are very similar to those displayed in the direct numerical simulations of § 3. For the clean interface shown in figure 7(*a*), the minimum or neck radius at $z = 0$ decreases monotonically in time, and the thread pinches off at $z = 0$ with a locally parabolic minimum, as is seen in the direct numerical simulation shown in figure 1.

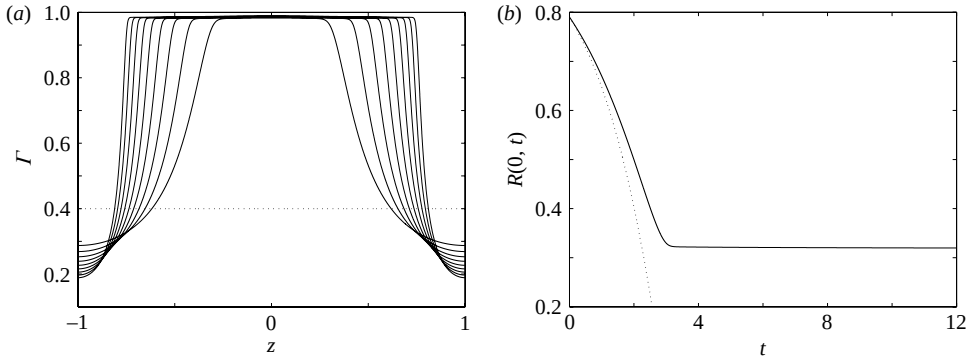

FIGURE 8. (*a*) Surfactant concentration $\Gamma(z,t)$ plotted at the same sequence of times as in figure 7(*b*). (*b*) Comparison of ϵ-scaled thread radius $R(z,t)$ at $z=0$ for a clean interface (dashed curve) with a surfactant coated interface (solid curve).

Figure 7(*b*) shows the evolution of the ϵ-scaled profile $R(z,t)$ when the interface is coated with a spatially uniform distribution of insoluble surfactant at $t=0$. This shows a similar evolution to that of the direct numerical simulations of § 3.2, that is, the profile first contracts radially to form a neck centred at $z=0$ and subsequently forms an elongated thread that connects parent bubbles centred at $z=\pm 1$. The distribution of surfactant Γ at the same sequence of times is shown in figure 8(*a*). Figure 8(*b*) shows the radius $R(0,t)$ versus time. The evolution is initially close to that of the clean surface but at time $t \simeq 3.0$, the decrease in the neck radius $R(0,t)$ is suddenly interrupted when the local decrease in area of the interface causes the surfactant concentration to approach its maximum value, and the data show that the neck radius remains almost steady thereafter. The surface tension σ on the thin thread is between 0.15 and 0.22.

The capillary pressure $p_c = \sigma/R$ balances the internal pressure p_i on the developing thin thread, and from (4.52) this part of the surface is stationary, which is in agreement with thread formation observed in the direct numerical simulations of § 3.2.

When $Pe_0 = \infty$, (4.54) simplifies to (4.59), so that ΓR is a function of z alone, independent of t. The initially uniform surfactant distribution Γ_i and almost uniform final surfactant distribution on the thin thread (figure 8*a*), imply that in the steady state the thin thread profile $R(z)$ is proportional to the initial profile $R(z,0)$. This imprint of the initial profile causes the concave upward shape of the steady thin thread in figure 7(*b*). In contrast, the simulations of § 3.2 for the same parameter values and initial surfactant concentration show a thread radius that decreases or constricts where the ends of the thread join the parent bubbles. This is seen in the data of figure 2 and was noted in the discussion of figure 4(*b*). This suggests that effects that are neglected in the leading-order long-wave equations, such as Marangoni stress and axial flow, decrease the accumulation of surfactant near the thread ends and facilitate the formation of constrictions. Surface diffusion of surfactant is an alternative mechanism that moderates localized accumulation of surfactant at the thread ends, and can readily be included in the long-wave model. In the next section, we investigate the effect of surface diffusion on a developing thread, and find that it leads to constrictions similar to those just described.

5.1.1. *The influence of surface diffusion*

Surface diffusion of surfactant is often neglected since its diffusivity is typically small. Consider a surfactant with a representative diffusivity $D_s = 10^{-5}$ cm^2 s^{-1} added

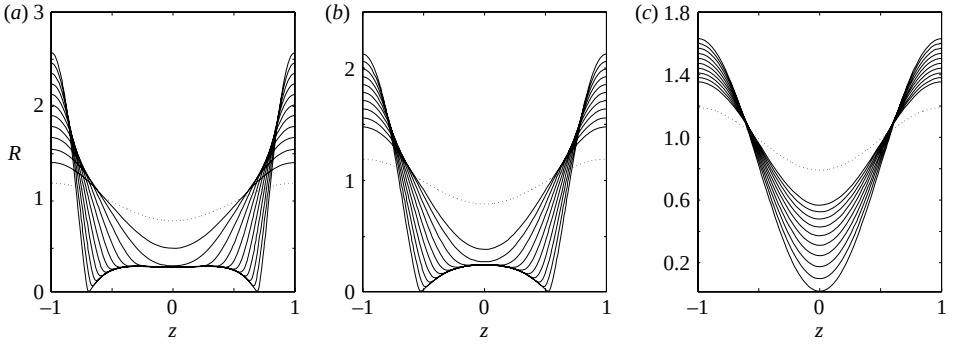

FIGURE 9. Long-wave evolution of a thread coated with surfactant that diffuses on its surface, with (*a*) $Pe_0 = 200$, (*b*) $Pe_0 = 50$, (*c*) $Pe_0 = 10$. The interfacial profiles are shown at $t = 0$ and from $t = 2$ to $t = 12$ in increments of $\Delta t = 1$ in (*a*), $t = 2.62$ to $t = 8.2$ in increments of $\Delta t = 0.62$ in (*b*), and $t = 1.4$ to $t = 3.2$ in increments of $\Delta t = 0.2$ in (*c*).

to glycerine with a clean surface tension in air of 63 dyn cm^{-1} and a viscosity of 14.9 dyn s cm^{-2}, so that the velocity scale $U = \sigma_0/\mu$ is of the order of 1 cms^{-1}. Then, assuming a length scale of 10^{-1} to 1 cm, the Péclet number Pe_s is in the range from 10^4 to 10^5. However, diffusive flux of surfactant has an effect on thread evolution, producing constrictions at the thread ends that are analogous to those observed in figure 2 and which eventually shrink to zero radius and pinch off.

For example, the evolution of a thread with the same initial data and parameter values as in figure 7(*b*), but with scaled Péclet number $Pe_0 = 200, 50$ and 10 is shown in figures 9(*a*) to (*c*), respectively. For $Pe_0 = 200$ and 50 in figures 9(*a*) and 9(*b*), the early evolution of the interface is similar to the diffusion-free case, with a fast radial collapse of an initial parabolic minimum followed by the formation of a thin thread in which the interior pressure and capillary pressure are equal. However, as the thread elongates, constrictions form at the thread ends and mark the onset of pinch-off. On the other hand, in figure 9(*c*), diffusion of surfactant is sufficiently large that the evolution closely resembles that of the clean or surfactant-free case.

The diffusive flux of surfactant on the thin thread of figures 9(*a*) and 9(*b*) is non-negligible only in a neighbourhood of the thread ends and on the parent bubble surface, as indicated in close-up in figure 10. The thread between the parent bubbles and away from its minimum radius is steady, as is shown in figure 9 and in greater detail in figure 10, and is concave downward, i.e. with constrictions at the thread ends.

This shape is a necessary consequence of the long-wave equations in the presence of surface diffusion. On steady parts of an interface, (4.54) simplifies to

$$\frac{\partial^2 \Gamma}{\partial z^2} + \frac{1}{R}\frac{\partial R}{\partial z}\frac{\partial \Gamma}{\partial z} = 0. \tag{5.1}$$

Since $\lambda_0 = 0$ and $p_i = p_i(t)$, differentiation of the steady version of (4.52) with respect to z gives

$$p_i \frac{\partial R}{\partial z} = \frac{\partial \sigma}{\partial \Gamma}\frac{\partial \Gamma}{\partial z}, \tag{5.2}$$

which, since $p_i > 0$ and $\partial_\Gamma \sigma < 0$, implies that $\partial_z R \partial_z \Gamma \leqslant 0$ and hence from (5.1) that $\partial_z^2 \Gamma_0 \geqslant 0$. Differentiating (5.2) with respect to z and recalling from the equation of state that $\partial_\Gamma^2 \sigma < 0$ then implies that $\partial_z^2 R \leqslant 0$ on steady parts of the thread.

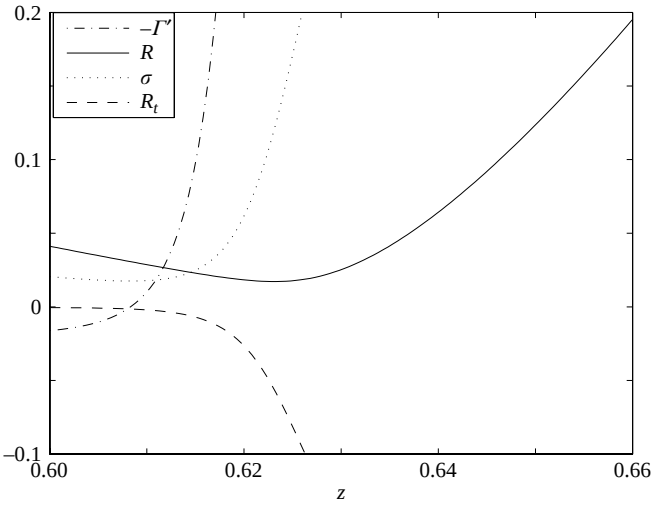

FIGURE 10. Close-up of the region where the thin thread of figure 9(*a*) connects to the parent bubble, indicating the formation of a constriction, for $Pe_0 = 200$. Shown are surface velocity $\partial_t R$, radius R, surface tension σ, and $-\Gamma'$ which is proportional to the diffusive flux of the surfactant.

Consequently, a non-uniform steady thread necessarily has a concave downward or spindle shape, as is observed for the thin thread in figures 9(*a*) and 9(*b*).

The surface tension σ is small in a neighbourhood of the constriction at the thread ends (see figure 10), and this brings into question the validity of the Langmuir equation of state in describing details of pinch-off. To model the equation of state for fluid systems at very high surfactant concentrations, as referred to in the discussion below (2.5), we have repeated the simulations of figures 9(*a*) and 9(*b*) with the modified equation of state

$$\sigma = \max(1 + E\ln(1-\Gamma), 0.1)\,. \tag{5.3}$$

As time proceeds, the lower bound on σ is first reached at the thin thread ends, where the surface tension is smallest. Thereafter, there is no qualitative difference in the evolution, but only a small, almost imperceptible, quantitative difference just before pinch-off. However, it is possible to prescribe initial conditions, parameter values and the lower bound so that the bound is first reached at the thread midpoint or neck $z = 0$, in which case the interface pinches off there without first forming a thin thread.

5.2. *A slightly viscous thread ($\lambda_0 > 0$)*

The evolution of a clean or surfactant-free interface for a slightly viscous thread with $\lambda = \epsilon^2\lambda_0$ has been thoroughly investigated in Sierou & Lister (2003), and here we summarize the main results. Figure 11(*a*) shows that the evolution of a clean surface when $\lambda_0 > 0$ is qualitatively similar to that when $\lambda_0 = 0$ only at sufficiently early times. The surface initially forms a minimum or neck at $z = 0$ which collapses radially; however, after some time, the velocity of the neck slows and subsequently changes sign, so that $R(0,t)$ increases for $t \gtrsim 4.8$. At this instant, there is a change in morphology from one to two minima, which are symmetric about $z = 0$ and simultaneously move toward the thread axis while translating away from $z = 0$. For a clean or surfactant-free interface, pinch-off occurs at finite time with a double-cone shape in the neighbourhood of a pinch point, as shown by a long-wave model and by

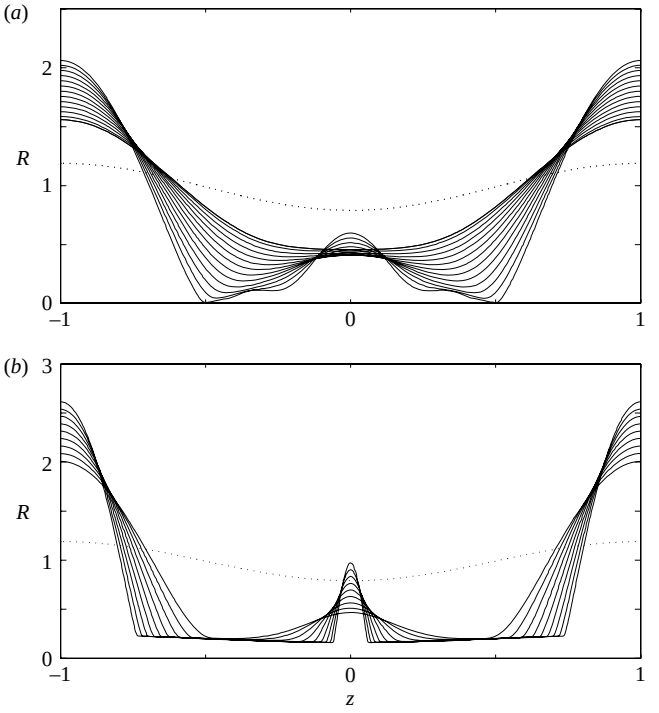

FIGURE 11. Numerical solutions of the long-wave equations for $\lambda_0 = 1$. The dotted line shows the initial interface profile. (*a*) Surfactant-free evolution; profiles are shown for $t = 0$ and from $t = 4.2$ to $t = 7.8$ in increments of $\Delta t = 0.3$, indicating that pinch-off first occurs near $z = \pm 0.5$ at the connection to the parent bubbles. (*b*) Evolution of the same initial profile coated with a uniform distribution of diffusion-free surfactant, with $\Gamma_i = 0.2$ and $E = 0.19$, showing a single satellite bubble separated from parent bubbles by quasi-steady thin threads. Times are $t = 0$ and from $t = 6$ to $t = 14$ in increments of $\Delta t = 1$.

similarity solutions of Stokes equations, without the approximations of the long-wave model, there being good quantitative agreement between the two approaches for sufficiently small λ (Sierou & Lister 2003).

An example of the evolution of a slightly viscous thread that is coated with diffusion-free insoluble surfactant is given in figure 11(*b*). The figure shows the interface $r = R(z, t)$ at a sequence of times for the same initial data as in figures 7(*b*) and 8, but with $\lambda_0 = 1$ and $\Gamma_i = 0.2$. The interface initially evolves as in the clean case, with a single neck at $z = 0$ that later divides into a symmetric pair of minima. However, as for an inviscid thread, the influence of surfactant is to interrupt the decrease in neck radius when the local interior pressure and capillary pressure balance, cf. (4.52), and a quasi-steady thin thread that connects a central satellite bubble forms along the axis of symmetry. In contrast to the inviscid case, satellite bubbles form owing to the spatial dependence of p_i, as specified by (4.53).

The additional effect of surface diffusion is illustrated in figure 12(*a*), which shows the profile $r = R(z, t)$ at a sequence of times using the same initial data as in figure 11(*b*), but with $Pe_0 = 200$. Figure 12(*b*) shows the corresponding surfactant concentration. As in the inviscid case, the diffusive flux of the surfactant is seen to promote the formation of constrictions at the ends of a steady thread, where it now joins either parent or satellite bubbles. The interface in figure 12(*a*) is first

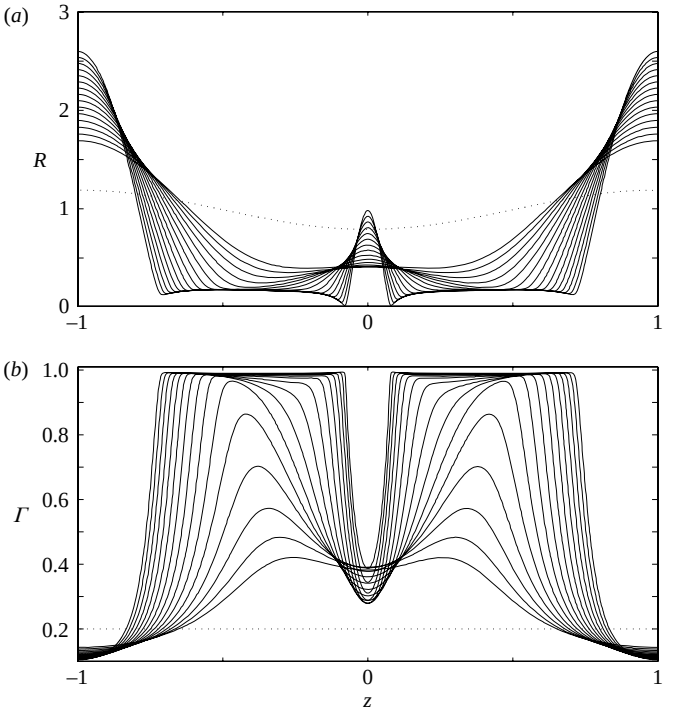

FIGURE 12. Numerical solution of the long-wave equations for $\lambda_0 = 1$, $Pe_0 = 200$, $E = 0.19$ and $\Gamma_i = 0.2$, plotted at $t = 0$ (dotted line) and from $t = 6.3$ to $t = 13.3$ in increments of 0.5. (*a*) Interface profiles $R(z, t)$ indicating pinch-off first occurs near $z = \pm 0.1$, away from the parent bubbles. (*b*) The corresponding surfactant concentration $\Gamma(z, t)$.

driven toward pinch-off at the point where the thread connects to the central satellite bubble rather than at the connection to the main parent bubbles as was found in the surfactant-free case of figure 11(*a*).

The result of (5.1) and (5.2), that the spindle shape of a steady thread is a necessary consequence of surface diffusion, extends to the case of a slightly viscous interior fluid provided $p_i' = 0$ at some point of it. This follows from (4.52) and (4.53), which imply that on intervals in z where the thread is steady, $(R^4 p_i')' = 0$ for all $\lambda_0 > 0$ and hence $R^4 p_i'$ is constant. Provided that $p_i' = 0$ at some point of the steady thread, such as near its mid-point, $p_i' = 0$ at all points along it, and the result then follows from the same reasoning as in the inviscid limit.

6. Numerical simulations revisited

A surprising prediction of the long-wave model is that since the Marangoni term, which appears in the tangential stress balance, decouples from the leading-order equations (4.52) to (4.55), the Marangoni stress is of reduced importance during the evolution of a slender bubble, and in particular in the formation of a thin quasi-steady thread. This prediction is examined in figure 13, which compares the evolution of a stretched bubble via direct numerical simulation with the Marangoni term included (dashed curve) and excluded or set to zero (solid curve), using similar initial data and the same parameter values as in the simulation of figure 2. The evolution is similar at early times in both cases, and, in particular, both show the formation of

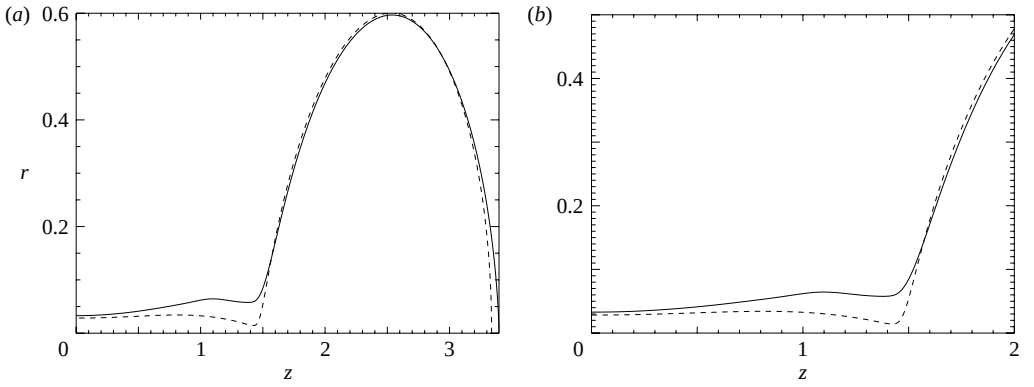

FIGURE 13. (*a*) Computed bubble profiles $r = R(z, t)$ both with (dashed curve) and without (solid curve) the Marangoni term. (*b*) Close-up of interface near the thread ends where the thread connects to the parent bubble, showing increased constriction in the presence of Marangoni stress.

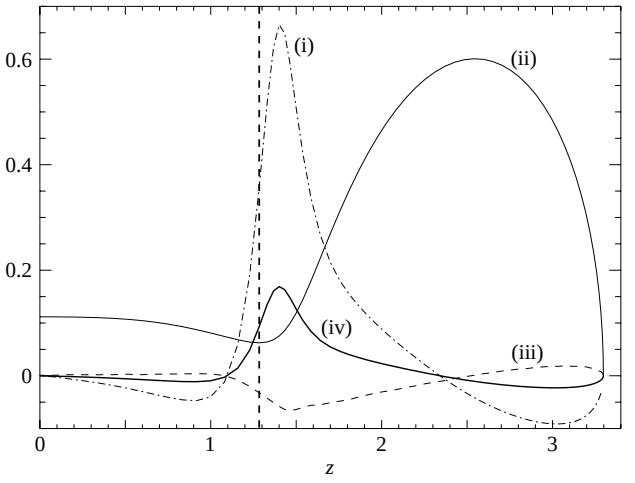

FIGURE 14. Spatial distribution of quantities from simulation of thread formation with initial surfactant coverage $\Gamma_i = 0.8$. Shown with the bubble profile $r = R(z, t)$ at $t = 11$ are: the surface tension gradient $\mathrm{d}\sigma/\mathrm{d}s$, the tangential velocity $\boldsymbol{u} \cdot \boldsymbol{t}$, and the bubble contraction rate $\partial R/\partial t$, scaled by suitable multiplying factors, as indicated. (i) $\mathrm{d}\sigma/\mathrm{d}s$; (ii) $R(z)$; (iii) $10\partial R/\partial t$; (iv) $40u_t$.

a persistent thin thread. However, the close-up of figure 13(*b*) shows that inclusion of the Marangoni stress has promoted the formation of a constriction at the thread ends, at which pinch-off will occur at some instant soon after that shown, whereas in the absence of Marangoni stress the constriction is absent and, with no surface diffusion, the profile shown is very near a final steady-state.

The above considerations motivate us to re-examine the dynamics in the neighbourhood of the constriction as the interface evolves according to the Navier–Stokes equations (2.1)–(2.7). A related investigation of the role of surfactant on thread evolution for a viscous thread in a passive surrounding is given by McGough & Basaran (2006). To facilitate the investigation here, the initial surfactant concentration is increased to $\Gamma_i = 0.8$, with the same initial bubble profile and other parameters as in § 3. The data in figure 14 show that away from the constriction at the thread

end, the thread surface is essentially steady and has a concave down or spindle-end shape. These features are reminiscent of the solution of the long-wave equations in the presence of surface diffusion of surfactant, see figure 9 and the discussion at (5.1) and (5.2). Figure 14 also shows that the tangential fluid velocity evaluated on the bubble surface and the Marangoni stress are largest in a localized neighbourhood of the constriction. This shows that either of these physical effects, both of which are neglected in the leading-order long-wave equations, act to sweep surfactant from the thread ends and onto the parent bubble in a manner analogous to the action of surface diffusion, thereby promoting pinch-off of the thread at its ends. A possible mechanism for the slow decrease in radius of the constriction is as follows: its axial propoagation rate $\dot{z}$ is approximately given by $\dot{z} = \partial_t R/R'$, where $\partial_t R$ follows approximately the same evolution for each slice of the thread. Since R' on the parent bubble adjacent to the constriction increases with time, $\dot{z}$ decreases with time. This gives more time for diffusion or Marangoni-induced flow to smooth the thread-drop surfactant gradient and reduce the effect of surfactant build-up at the constriction.† We expect that the effects of Marangoni stress and tangential velocity on the interface can be investigated by including higher-order terms in the long-wave model, but do not pursue this here.

Figure 15 shows simulation data for a range of different initial values of surfactant concentration Γ_i and illustrates the influence this has on thread formation. The same initial bubble shape as in § 3 is adopted, see figure 1(*a*), with other parameter values as in figures 2 to 5.

During the initial stage of evolution, bubble contraction in the vicinity of $z = 0$ occurs, with an increase in local surfactant concentration due to the decrease in surface area. However, the greater the initial surfactant concentration, the more readily the capillary pressure approaches the interior pressure, so that the quasi-steady thread radius is seen in figure 15(*a*, *b*) to be larger at increased initial concentration Γ_i. The surface tension shown in figure 15(*c*) is 0.2 or larger on the thin thread, except at the constrictions. The corresponding surfactant distribution is shown in figure 15(*d*).

7. Conclusion

Novel bubble dynamics, such as tip-streaming in an extensional flow, and drag enhancement in an axisymmetric translational flow is often associated with the influence of surfactant. Here, we have investigated the evolution toward pinch-off of a slender, axisymmetric prestretched bubble with insoluble surfactant in a quiescent flow. The results of direct numerical simulation for an inviscid bubble show that in contrast to the surfactant-free or clean case, in which the bubble pinches off with a parabolic profile at the same location as a minimum of the initial radius, the influence of the surfactant is to interrupt the event of pinch-off when the minimum radius is a fraction of its initial value. The radius at interruption varies with the amount of surfactant present at the initial instant, Γ_i, from about 35% of its initial value when $\Gamma_i \simeq 0.4$ to 50% at $\Gamma_i \simeq 0.6$ (see figure 15*a*). Instead of pinch-off, a thin quasi-steady thread develops, centred on this location and with a near-constant radius, and then elongates until its aspect ratio is approximately 0.035–0.07 when it separates two distinct parent bubbles at its ends. The presence of singular terms near pinch-off in an axisymmetric geometry, for example, the capillary pressure σ/R, implies a loss of accuracy in the computations when the radius is less than $10^{-3} - 10^{-4}$.

† We thank a referee for pointing this out.

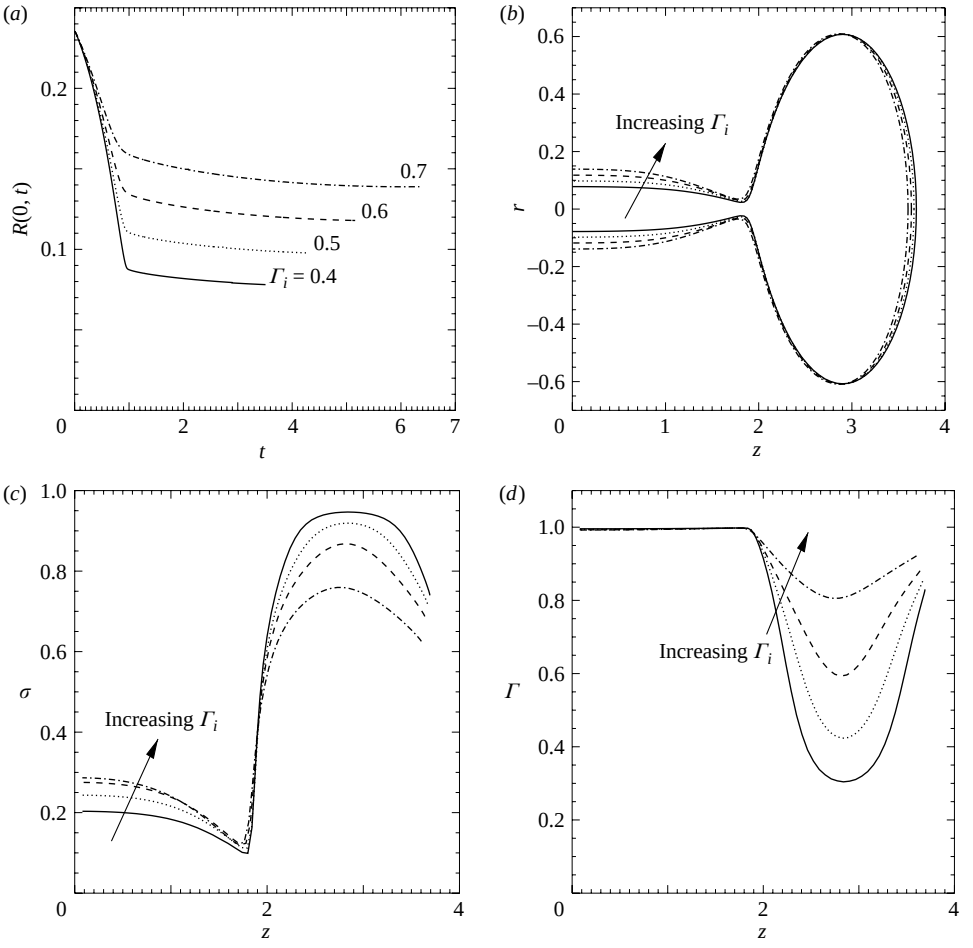

FIGURE 15. Evolution for different values of the initial surfactant coverage Γ_i: $\Gamma_i = 0.4$ (solid line), $\Gamma_i = 0.5$ (dotted line), $\Gamma_i = 0.6$ (dashed line), $\Gamma_i = 0.7$ (dash-dotted line). (*a*) Thread radius $R(0, t)$ at $z = 0$ versus time t. (*b*) Bubble profile $r = R(z, t)$ at large time, equal to the latest time shown for each Γ_0 in (*a*). (*c*) Surface tension $\sigma(z, t)$ at the same large time. (*d*) Surfactant concentration $\Gamma(z, t)$ at the same large time.

The direct numerical simulations are augmented by a long-wave asymptotic model for the evolution of a thread. The code used for the direct numerical simulations in this paper does not include non-zero viscosity of the interior fluid. The influence of interior viscosity can, however, readily be incorporated into a long-wave asymptotic model in the zero-Reynolds-number or Stokes-flow limit, and this identifies the dominant physical mechanisms responsible for the thread's formation and evolution.

Unlike previous examples (Pawar & Stebe 1996; Eggleton, Pawar & Stebe 1999; Wang, Papageorgiou & Maldarelli 1999; Booty & Siegel 2005; Li 2006) in which Marangoni stress is essential to novel surfactant-induced dynamics, surfactant-induced thread formation in the process of bubble contraction is due primarily to normal stress-balance and is therefore not a consequence of Marangoni stress. This is illustrated by both direct numerical simulation and the longwave asymptotic model, which shows that Marangoni stress does not play a role in the leading-order dynamics of thread formation. During the evolution, surfactant concentration

increases, owing to the contraction or decrease in local surface area of the bubble interface, thereby reducing surface tension and establishing a near-balance between the capillary pressure and internal bubble pressure. This results in the formation of a quasi-steady thin thread, which then elongates to join a pair of slowly contracting parent bubbles.

In the direct numerical simulations, the elongating thread develops a spindle shape or constricts at its ends where it joins the parent bubbles. The high concentration of surfactant on the thread and relatively low concentration on the adjacent parent bubble imply the presence of a Marangoni stress that is localized about the constriction at the thread end and is accompanied by a surface-tangential velocity. The tangential velocity gives rise to localized advection of surfactant from the thread, with its high surfactant concentration, to the parent bubble, with its relatively low surfactant concentration. As surfactant leaves the end of the thread and enters the parent bubble surface, the radius at the end of the thread decreases to establish a balance between capillary and internal pressure. This is the mechanism that leads to the formation of a constriction between the end of the thread and the parent bubble, and while the thread elongates and the radius at the constriction decreases, the remainder of the thread remains in quasi-steady equilibrium. This Marangoni stress-induced surfactant transport from the thread end to the parent bubble causes the constriction to decrease until the thread is eventually driven to pinch-off there.

In the absence of Marangoni stress and tangential surface velocity, both of which are shown in § 4 to be higher-order effects in the long-wave model, surface diffusion of surfactant can also lead to the development of a spindle-shaped thread and eventual pinch-off at its ends provided the diffusivity is sufficiently small but non-zero. We therefore conclude that pinch-off at the end of an inviscid thread is unavoidable in the presence of surfactant transport away from the thread, whether it occurs by Marangoni-induced advection or surface diffusion.

When the interior fluid has small but non-zero viscosity, the long-wave model indicates that the quasi-steady thread is punctuated by satellite bubbles that can form along its length. The quasi-steady portions of the slender thread can then first approach pinch-off adjacent to a satellite bubble instead of a parent bubble.

It is important to note the different role played by surfactant in the evolution toward pinch-off of a thread as the viscosity ratio $\lambda = \mu_i/\mu$ varies from the small values considered here to larger values. Timmermans & Lister (2002) derive a long-wave model for a viscous thread with $\lambda = \infty$ in a passive surrounding, and show that in the absence of surface diffusion it predicts that the extensional flow away from the point of pinch-off advects surfactant away from the region, with the result that surfactant has a negligible effect on the dynamics close to pinch-off. The different behaviour found here is due mainly to the difference in the form of the lubrication-type velocity profile within the thread. When $\lambda \gg 1$ or $\lambda = \infty$, the thread velocity profile is plug-like, so that the axial flow near pinch-off causes a tangential velocity at the interface that is of the same magnitude as the flow at all points across the thread. On the other hand, when $\lambda \ll 1$, the profile is of Poiseuille type, so that near pinch-off the axial flow is greatest on the thread axis and is small at the interface, thereby relegating the role of advection of surfactant along the interface and away from the pinch-off region to higher order. More precisely, we find that with the scaling $\lambda \sim \epsilon^2$, when the radial velocity at the interface is $O(1)$ the axial velocity is small, $O(\epsilon \ln(1/\epsilon))$, and the leading-order long-wave model predicts that the surfactant concentration becomes sufficiently large that the surface tension is greatly reduced as pinch-off occurs.

The authors thank Charles Maldarelli for extensive discussions on this work. The work of D.T.P. was supported by NSF grant DMS-0072228, and that of M.R.B., M.S. and Y.N.Y. by NSF grant DMS-0708977. Additional support was provided by a NJIT/SBR grant (to Y.N.Y.), and by NSF grant DMS-0354560 (to M.S.). The simulations were conducted on the NJIT computing cluster supported by NSF/MRI grant number DMS-0420590.

REFERENCES

Acrivos, A. & Lo, T. S. 1978 Deformation and breakup of a single slender drop in an extensional flow. *J. Fluid Mech.* **86**, 641–672.

Ambravaneswaran, B. & Basaran, O. A. 1999 Effects of insoluble surfactants on the nonlinear deformation and breakup of stretching liquid bridges. *Phys. Fluids* **11** (5), 997–1015.

Anna, S. L. & Mayer, H. C. 2006 Microscale tipstreaming in a microfluidic flow focusing device. *Phys. Fluids* **18**, 121512.

Basaran, O. A. 2002 Small-scale free surface flows with breakup: drop formation and emerging applications. *AIChE J.* **48**, 1842–1848.

Belytschko, T., Kennedy, J. M. & Schoeberle, D. F. 1980 Quasi-Eulerian finite element formulation for fluid–structure interaction. *Trans. ASME J. Press. Vessel Technol.* **102**, 62–69.

Booty, M. R. & Siegel, M. 2005 Steady deformation and tip-streaming of a slender bubble with surfactant in extensional flow. *J. Fluid Mech.* **544**, 243–275.

Brenner, M. P., Lister, J. R. & Stone, H. A. 1996 Pinching threads, singularities and the number 0.0304... *Phys. Fluids* **8** (11), 2827–2836.

Buckmaster, J. D. 1972 Pointed bubbles in slow viscous flow. *J. Fluid Mech.* **55**, 385–400.

Burkholder, H. C. & Berg, J. C. 1974 Effect of mass transfer on laminar jet breakup. Part I: liquid jets in gases. Part II: liquid jets in liquids. *AIChE J.* **20**, 863–880.

Chang, C.-H. & Franses, E. I. 1995 Adsorption dynamics of surfactants at the air/water interface: a critical review of mathematical models, data and mechanisms. *Colloids Surfaces* A **100**, 1–45.

Craster, R. V., Matar, O. K. & Papageorgiou, D. T. 2002 Pinchoff and satellite formation in surfactant covered viscous threads. *Phys. Fluids* **14** (4), 1364–1376.

De Bruijn, R. A. 1993 Tipstreaming of drops in simple shear flows. *Chem. Engng. Sci.* **48**, 277–284.

Donea, J., Giuliani, S. & Halleux, J. P. 1982 An arbitrary Lagrangian–Eulerian finite element method for transient dynamic fluid structure interaction. *Comput. Meth. Appl. Mech. Engng* **33**, 689–723.

Donea, J. & Huerta, A. 2003 *Finite Element Methods for Flow Problems*. Wiley.

Doshi, P., Cohen, I., Zhang, W. W., Siegel, M., Howell, P., Basaran, O. A. & Nagel, S. R. 2003 Persistence of memory in drop breakup: the breakdown of universality. *Science* **302**, 1185–1188.

Eggers, J. 1993 Universal pinching of 3D axisymmetric free-surface flow. *Phys. Rev. Lett.* **71**, 3458–3464.

Eggers, J. 1995 Theory of drop formation. *Phys. Fluids* **7**, 941–953.

Eggers, J. 1997 Nonlinear dynamics and breakup of free-surface flows. *Rev. Mod. Phys.* **69**, 865–929.

Eggers, J. & Dupont, T. F. 1994 Drop formation in a one-dimensional approximation of the Navier–Stokes equation. *J. Fluid Mech.* **262**, 205–221.

Eggleton, C. D., Pawar, Y. P. & Stebe, K. J. 1999 Insoluble surfactants on a drop in an extensional flow: a generalization of the stagnated surface limit to deforming interfaces. *J. Fluid Mech.* **385**, 79–99.

Handelsman, R. A. & Keller, J. B. 1967 Axially symmetric potential flow around a slender body. *J. Fluid Mech.* **28**, 131–147.

Hansen, S., Peters, G. W. M. & Meijer, H. E. H. 1999 The effect of surfactant on the stability of a fluid filament embedded in a viscous fluid. *J. Fluid Mech.* **382**, 331–349.

Hinch, E. J. 1991 *Perturbation Methods*. Cambridge University Press.

Hirt, C. W., Amsden, A. A. & Cook, J. L. 1974 An arbitrary Lagrangian–Eulerian computing method for all flow speeds. *J. Comput. Phys.* **14**, 227–253 (Reprinted in *J. Comput. Phys.* **135**(2), 203–216, 1997).

Janssen, J. J. M., Boon, A. & Agterof, W. G. M. 1994 Influence of dynamic interfacial properties on droplet breakup in simple shear flow. *AIChE. J.* **40**, 1929–1939.

Janssen, J. J. M., Boon, A. & Agterof, W. G. M. 1997 Influence of dynamic interfacial properties on droplet breakup in plane hyperbolic flow. *AIChE. J.* **43**, 1436–1447.

Jin, F., Gupta, N. R. & Stebe, K. J. 2006 The detachment of a viscous drop in a viscous solution in the presence of a soluble surfactant. *Phys. Fluids* **18**, 022103.

Kwak, S. & Pozrikidis, C. 2001 Effect of surfactants on the instability of a liquid thread or annular layer. Part I. quiescent fluids. *Int. J. Multiphase Flow* **27**, 1–37.

Li, J. 2006 The effect of an insoluble surfactant on the skin friction of a bubble. *Eur. J. Mech.* B *Fluid* **25**, 59–73.

Li, J., Hesse, M., Ziegler, J. & Woods, A. W. 2005 An arbitrary Lagrangian Eulerian method for moving-boundary problems and its application to jumping over water. *J. Comput. Phys.* **208**, 289–314.

Liao, Y.-C., Franses, E. I. & Basaran, O. A. 2006 Deformation and breakup of a stretching liquid bridge covered with an insoluble surfactant monolayer. *Phys. Fluids* **18** (2), 022101.

Lister, J. R. & Stone, H. 1998 Capillary breakup of a viscous thread surrounded by another viscous fluid. *Phys. Fluids* **10** (11), 2758–2764.

McGough, P. T. & Basaran, O. A. 2006 Repeated formation of fluid threads in breakup of a surfactant-covered jet. *Phys. Rev. Lett.* **96**, 054502–1–054502–4.

Milliken, W. J., Stone, H. A. & Leal, L. G. 1993 The effect of surfactant on the transient motion of Newtonian drops. *Phys. Fluids* **5** (1), 69–79.

Notz, P. K., Chen, A. U. & Basaran, O. A. 2001 Satellite drops: unexpected dynamnics and change of scaling during pinch-off. *Phys. Fluids* **13** (3), 549–552.

Papageorgiou, D. T. 1995 On the breakup of viscous liquid threads. *Phys. Fluids* **7** (7), 1529–1544.

Pawar, Y. & Stebe, K. J. 1996 Marangoni effects on drop deformation in an extensional flow: the role of surfactant physical chemistry. I. Insoluble surfactants. *Phys. Fluids* **8** (7), 1738–1751.

Quéré, D. 1999 Fluid coating on a fiber. *Annu. Rev. Fluid Mech.* **31**, 347–384.

Rayleigh, Lord 1879 On the instability of jets. *Proc. Lond. Math. Soc.* **10**, 4.

Rayleigh, Lord 1892 On the stability of a cylinder of viscous liquid under capillary force. *Phil. Mag.* **34**, 145.

Rothert, A., Richter, R. & Rehberg, I. 2001 Transition from symmetric to axisymmetric scaling function before drop pinch-off. *Phys. Rev. Lett.* **87**, 0845501.

Ryskin, G. & Leal, L. G. 1984 Numerical solution of free-boundary problems in fluid mechanics. Part 1. The finite-difference technique. *J. Fluid Mech.* **148**, 1–17.

Sierou, A. & Lister, J. R. 2003 Self-similar solutions for viscous capillary pinch-off. *J. Fluid Mech.* **497**, 381–403.

Stone, H. A. 1994 Dynamics of drop deformation and breakup in viscous fluids. *Annu. Rev. Fluid Mech.* **26**, 65–102.

Stone, H. A. & Leal, L. G. 1990 The effects of surfactants on drop deformation and breakup. *J. Fluid Mech.* **220**, 161–186.

Suryo, R., Doshi, P. & Basaran, O. A. 2004 Non-self-similar, linear dyanmics during pinch-off of a hollow annular jet. *Phys. Fluids* **16**, 4177.

Taylor, G. I. 1964 Conical free surfaces and fluid interfaces. In *Proc. 11th Intl. Cong. Theor. Appl. Mech. (Munich 1964)*, pp. 790–796. Springer.

Timmermans, M.-L. E. & Lister, J. R. 2002 The effect of surfactant on the stability of a liquid thread. *J. Fluid Mech.* **459**, 289–306.

Tomotika, S. 1935 On the instability of a cylindrical thread of a viscous liquid surrounded by another viscous fluid. *Proc. R. Soc. Lond.* A **150**, 322–337.

Wang, Y., Papageorgiou, D. & Maldarelli, C. 1999 Increased mobility of a surfactant-retarded bubble at high bulk concentrations. *J. Fluid Mech.* **390**, 251–270.

Whitaker, S. 1976 Studies of the drop-weight method for surfactant solutions: III. Drop stability, the effect of surfactants on the stability of a column of liquid. *J. Colloid Interface Sci.* **54**, 231–248.

Wilkes, E. D., Phillips, S. D. & Basaran, O. A. 1999 Computational and experimental analysis of dynamics of drop formation. *Phys. Fluids* **11** (12), 3577–3598.

Wong, H., Rumschitzki, D. & Maldarelli, C. 1996 On the surfactant mass balance at a deforming fluid interface. *Phys. Fluids* **8** (11), 3202–3204.

Zhang, W. W. & Lister, J. R. 1999 Similarity solutions for capillary pinch-off in fluids of differing viscosity. *Phys. Rev. Lett*. **83** (6), 1151–1154.

Zhang, X. & Basaran, O. A. 1995 An experimental study of dynamics of drop formation. *Phys. Fluids* **7** (6), 1184–1203.